Chinese Journal of Natural Medicines

Hyperperins AX, fusicoccane diterpenoids including an unreported 5/7/5/3 tetracyclic carbon skeleton from *Hypoestes purpurea* and their T-type calcium channel inhibitory activity

Linfen Ding, Ming Hu, Qiaoling Wei, Shihuan Yin, Xinying Wang, Lu Sai, Wenyan Li, Xingde Wu

Citation: Linfen Ding, Ming Hu, Qiaoling Wei, Shihuan Yin, Xinying Wang, Lu Sai, Wenyan Li, Xingde Wu, Hyperperins AX, fusicoccane diterpenoids including an unreported 5/7/5/3 tetracyclic carbon skeleton from *Hypoestes purpurea* and their T-type calcium channel inhibitory activity, Chinese Journal of Natural Medicines, 2026, 24(10), 1262-1280. doi: 10.1016/S1875-5364(26)61219-8.

View online: https://doi.org/10.1016/S1875-5364(26)61219-8

Related articles that may interest you

Glasesterterpenoids AC: three sesterterpenoids with 7-cyclohexyldecahydronaphthalene carbon skeleton isolated from the root of *Lindera glauca*

Chinese Journal of Natural Medicines. 2024, 22(9), 864-868 https://doi.org/10.1016/S1875-5364(24)60657-6

New tirucallane-type triterpenoids from the resin of *Boswellia carterii* and their NO inhibitory activities

Chinese Journal of Natural Medicines. 2021, 19(9), 686-692 https://doi.org/10.1016/S1875-5364(21)60099-7

New pimarane diterpenoids with antibacterial activity from fungus *Arthrinium* sp. ZS03

Chinese Journal of Natural Medicines. 2024, 22(4), 356-364 https://doi.org/10.1016/S1875-5364(24)60629-1

Lignans with NO inhibitory activity from *Tinospora sinensis*

Chinese Journal of Natural Medicines. 2021, 19(7), 500-504 https://doi.org/10.1016/S1875-5364(21)60049-3

New *nor-ent*-halimane and *nor*-clerodane diterpenes from *Callicarpa integerrima* with anti-MRSA activity

Chinese Journal of Natural Medicines. 2024, 22(11), 1003-1010 https://doi.org/10.1016/S1875-5364(24)60575-3

Antimalarial and neuroprotective *ent*-abietane diterpenoids from the aerial parts of *Phlogacanthus curviflorus*

Chinese Journal of Natural Medicines. 2023, 21(8), 619-630 https://doi.org/10.1016/S1875-5364(23)60464-9

Wechat

Chinese Journal of Natural Medicines 24 (2026) 1262-1280

Contents lists available at ScienceDirect

Chinese Journal of Natural Medicines

journal homepage: www.cjnmcpu.com/



Original article

Hyperperins A–X, fusicoccane diterpenoids including an unreported 5/7/5/3 tetracyclic carbon skeleton from *Hypoestes purpurea* and their T-type calcium channel inhibitory activity

Linfen Ding[a,b,Δ], Ming Hu[a,Δ], Qiaoling Wei[a], Shihuan Yin[a,b], Xinying Wang[a,b], Lu Sai[a,b], Wenyan Li[c,*], Xingde Wu[a,*]

[a] *Key Laboratory of Ethnic Medicine Resource Chemistry, Ministry of Education, Yunnan Minzu University, Kunming 650504, China*
[b] *School of Pharmaceutical Sciences & Yunnan Key Laboratory of Pharmacology for Natural Products, Kunming Medical University, Kunming 650500, China*
[c] *State Key Laboratory of Phytochemistry and Natural Medicines, Kunming Institute of Botany, Chinese Academy of Sciences, Kunming 650201, China; University of Chinese Academy of Sciences, Beijing 100049, China*

ARTICLE INFO

Article history:
Received 7 April 2026
Revised 12 August 2026
Accepted 14 August 2026
Available online 20 October 2026

Keywords:
Hypoestes purpurea
Fusicoccane diterpenoids
$Ca_v3.1$ calcium channel inhibitory activities

ABSTRACT

Two unprecedented rearranged fusicoccane diterpenoids, hyperperins A (**1**) and B (**2**), and twenty-two new fusicoccane diterpenoids, hyperperins C–X (**3–24**), were isolated from the aerial parts of *Hypoestes purpurea*, as well as one known analog (**25**). The structures and absolute configurations of all newly isolated compounds were determined through comprehensive analyses, including NMR spectroscopy, HR-ESI-MS, electronic circular dichroism calculations, and single-crystal X-ray diffraction analysis. Structurally, compounds **1** and **2** were characterized by a previously unreported carbon skeleton featuring a 5/7/5/3 tetracyclic ring system. Compounds **19** and **20** represent the first examples of fusicoccane diterpenoids with epoxy groups at C-2/C-6 and C-6/C-7, respectively. A plausible biosynthesis pathway for compounds **1** and **2** was proposed. Additionally, compounds **1**, **2**, **3**, **7**, and **25** exhibited potent inhibitory activity against the $Ca_v3.1$ calcium channel with IC_{50} values of 15.06 ± 1.19, 9.00 ± 1.04, 6.04 ± 0.67, 14.00 ± 1.20, and 6.26 ± 0.82 μmol·L^{-1}, respectively. These findings enrich the structural diversity of fusicoccane diterpenoids and provide promising lead compounds for the development of $Ca_v3.1$ calcium channel inhibitors.

1. Introduction

Ion channels are a class of transmembrane proteins that form pores and play a crucial role in maintaining normal physiological functions in the human body [1, 2]. Structural alterations or functional impairments of these channels can lead to serious cardiovascular diseases, neurological disorders, pain syndromes, and even malignancies [3-7]. Among currently available therapeutic drugs, those targeting ion channels account for 19% of the total, second only to drugs targeting G-protein-coupled receptors [8]. With the rapid development of electrophysiological techniques and the application of high-throughput ion channel drug screening, an increasing number of novel ion channel modulators have entered clinical trials and reached the market. Notable examples include ivabradine, an inhibitor of hyperpolarization-activated cyclic nucleotide-gated (HCN) channels used to treat chronic heart failure; amantadine, an *N*-methyl-D-aspartic acid (NMDA) receptor antagonist employed in the management of Parkinson's disease; and brexanolone, a positive allosteric modulator of the γ-aminobutyric acid type A ($GABA_A$) receptor, approved for the treatment of post-partum depression [9].

T-type calcium channels, also known as low-voltage-activated calcium channels, are important members of the voltage-gated calcium channel family [10-12]. This channel family comprises three subtypes, namely $Ca_v3.1$, $Ca_v3.2$, and $Ca_v3.3$, which are encoded by the α_1 subunit genes *CACNA1G*, *CACNA1H*, and *CACNA1I*, respectively [13, 14]. T-type calcium channels are primarily expressed in neurons and cardiomyocytes, and their functional dysregulation is closely associated with the pathogenesis of neurological and cardiovascular diseases [11, 15-17]. Mounting evidence indicates that T-type calcium channels exhibit considerable potential in regulating neurological functions and have become important targets for the development of therapeutic drugs for epilepsy, neuropathic pain, parkinsonism, and other disorders [14, 17-19]. Natural products play a pivotal role in the research and development of ion channel-targeting therapeutics, as demonstrated by classic examples such as lidocaine, amiodarone, and verapamil [9]. In recent years, the discovery of novel natural products with ion channel-modulating activities has become a rapidly advancing area of investigation. Notably, several T-type calcium channel inhibitors have also been identified from natural resources, including the meroterpenoid (+)-cochlearoid A isolated from *Ganoderma cochlear* [20]; the dearomatized isoprenylated acylphloroglucinol hypatone A obtained from *Hypericum patulum* [21]; and the indole alkaloid rhynchine A derived from *Uncaria rhynchophylla* [22].

* Corresponding author.
E-mail addresses: liwenyan@mail.kib.ac.cn (W. Li); wuxingdeymu@163.com (X.Wu)
Δ These authors contributed equally to this work.

https://doi.org/10.1016/S1875-5364(26)61219-8
Copyright © 2026, China Pharmaceutical University. Published by Elsevier B.V. All rights are reserved.

Hypoestes purpurea (L.) R. Br., a species within the genus *Hypoestes* of the Acanthaceae family, is native to regions including Guangxi, Guangdong, Hainan, Taiwan, and the Philippines. Traditionally, this plant has been used to treat tuberculosis, hemoptysis, bronchitis, diabetes, and traumatic injuries [23]. Previous phytochemical studies on the genus *Hypoestes* have revealed the presence of structurally diverse labdane, fusicoccane, and verticillane diterpenoids, many of which exhibit potent cytotoxic, anti-inflammatory, vasorelaxant, antifungal, and antiplasmodial activities [24-34]. However, the chemical constituents of *H. purpurea* have been scarcely studied, with only a few labdane-type and fusicoccane diterpenoids reported, such as hypopurin A and hypoestin D [24, 28]. As part of our ongoing research on the discovery of bioactive diterpenoids from the genus *Hypoestes*, two rearranged fusicoccane diterpenoids with a new carbon skeleton, hyperperins A and B (**1** and **2**), featuring a unique 5/7/5/3 ring system, were isolated from the aerial parts of *H. purpurea*. Additionally, twenty-two new fusicoccane diterpenoids, hyperperins C–X (**3–24**), and one known fusicoccane diterpenoid, fusicocc-4(16), 8(9)-dien-14-one (**25**) [25], were obtained (Fig. 1). Presented herein are the isolation, structural elucidation, and T-type calcium channel inhibitory activities of these compounds, as well as a plausible biosynthetic pathway for compounds **1** and **2**.

2. Results and discussion

2.1. Structural identification

Two novel fusicoccane diterpenoids, hyperperins A and B (**1** and **2**), featuring a unique 5/7/5/3 fused carbon ring system, were isolated from the aerial parts of *H. purpurea*. In addition, twenty-two new fusicoccane diterpenoids, hyperperins C–X (**3–24**), along with one previously identified congener, fusicocc-4(16),8(9)-dien-14-one (**25**), were also obtained (Fig. 1).

Hyperperin A (**1**) was obtained as a white amorphous powder and determined to have the molecular formula $C_{20}H_{28}O$, as established by HR-ESI-MS analysis (*m/z* 307.2030 $[M + Na]^+$, Calcd. for 307.2032), suggesting seven degrees of unsaturation. The IR spectrum exhibited characteristic absorption bands corresponding to olefinic (1627 cm^{-1}) and ketone carbonyl (1739 cm^{-1}) groups. The ^1H NMR data (Table 1) revealed the presence of three methyl groups, including one singlet at δ_H 0.95 and two doublets at δ_H 0.94 (J = 6.6 Hz) and δ_H 0.83 (J = 6.6 Hz), two exocyclic double bonds with geminal protons at δ_H 4.79 (d, J = 2.1 Hz), 4.73 (d, J = 2.1 Hz), and δ_H 4.97 (d, J = 3.5 Hz), 4.87 (d, J = 3.5 Hz). The ^{13}C NMR and DEPT spectra of **1** (Table 2) displayed 20 carbon resonances, which were assigned to three methyl carbons, seven methylene carbons including two olefinic carbons at δ_C 105.8 and 113.4, five methine carbons, and five nonprotonated carbons consisting of one ketone carbonyl carbon (δ_C 224.4), two aliphatic carbons (δ_C 35.1, 52.4), and two olefinic carbons (δ_C 157.2, 149.8). The presence of one carbonyl group and two double bonds accounts for three out of the seven degrees of unsaturation, suggesting that **1** is a diterpenoid featuring a fused tetracyclic ring system.

The planar structure of **1** was elucidated through the interpretation of the ^1H–^1H COSY and HMBC spectra. The ^1H–^1H COSY spectrum (Fig. 2) revealed the presence of the three spin systems: –CH_2-CH-CH-CH_2-CH_2– (for C-1/C-2/C-6/C-5/C-4), –CH-CH_2– (for C-8/C-9), and CH_3-CH(CH_3)-CH-CH_2– (for C-20/C-15(C-19)/C-14/C-13. HMBC correlations (Fig. 2) from H_2-16 (δ_H 4.79, d, J = 2.1 Hz; 4.73, d, J = 2.1 Hz) to C-2 (δ_C 46.1), C-3 (δ_C 157.2) and C-4 (δ_C 31.9) confirmed the formation of a five-membered ring A bearing an exocyclic $\Delta^{3,16}$ double bond. HMBC correlations from H_2-17 (δ_H 4.97, d, J = 3.5 Hz; 4.87, d, J = 3.5 Hz) to C-6 (δ_C 48.7),

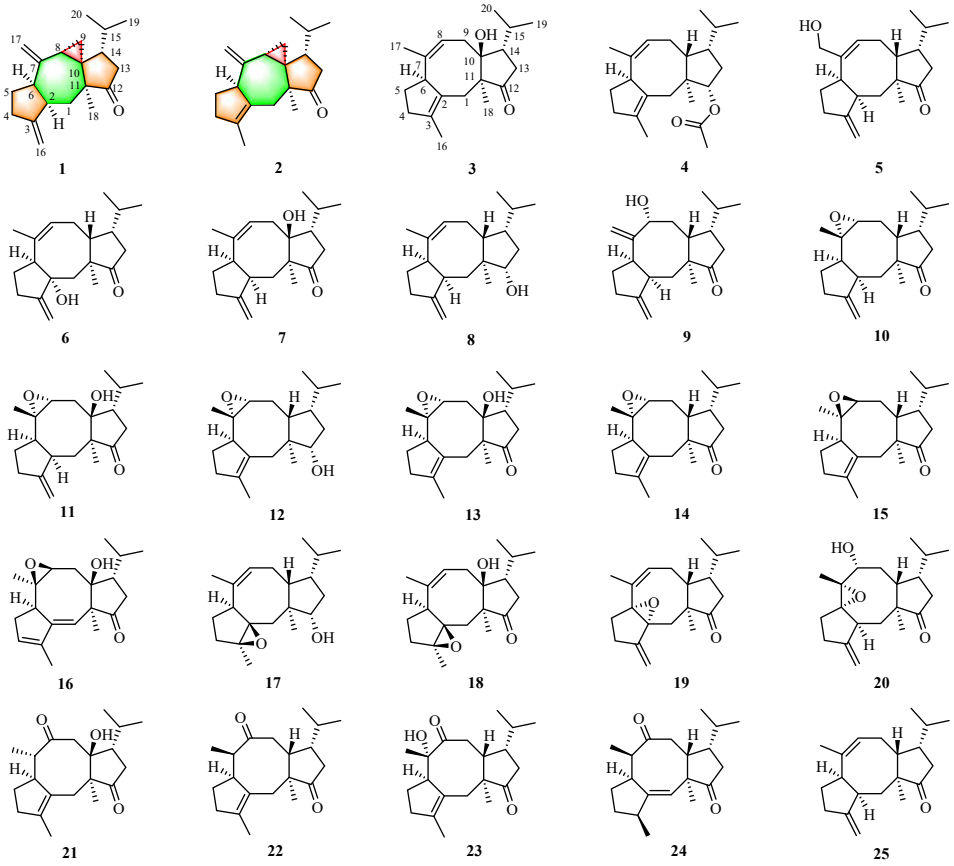


Fig. 1 Structures of compounds **1–25**.

Table 1 ^{1}H (500 MHz) NMR spectroscopic data of **1**–**6** (*J* in Hz).

Position	**1**[a]	**2**[b]	**3**[b]	**4**[a]	**5**[b]	**6**[b]
1a	1.68, t (13.9)	2.45, d (13.9)	2.59, d (15.1)	2.44, d (14.1)	2.25, dd (14.0, 4.2)	2.74, d (14.8)
1b	1.34, dd (13.9, 4.6)	1.79, d (13.9)	1.94, d (15.1)	1.51, d (14.1)	0.82, dd (14.0, 11.7)	1.37, d (14.8)
2	2.59, m				2.54, m	
4a	2.48, m	2.29, m	2.30, m	2.31, m	2.49, m	2.54, m
4b	2.36, m	2.21, m	2.30, m	2.31, m	2.37, m	2.35, m
5a	1.81, m	1.90, m	1.84, m	1.87, m	2.03, m	2.08, m
5b	1.94, m	1.80, m	1.84, m	1.82, m	1.85, m	1.56, m
6	2.70, dd (15.4, 7.3)	3.19, m	3.66, m	3.71, m	3.37, m	2.81, dd (12.7, 6.0)
8	1.62, dd (9.1, 5.7)	1.63, dd (9.2, 6.7)	5.44, dd (9.7, 8.1)	5.53, t, 8.1	5.83, t, 8.2	5.65, t (8.0)
9a	1.07, dd (9.1, 5.7)	1.06, dd (9.2, 5.6)	2.85, dd (13.7, 8.1)	2.37, ddd (13.6, 10.5, 8.1)	2.54, m	2.48, m
9b	1.01, t (5.7)	0.92, dd (6.7, 5.6)	2.44, dd (13.7, 9.7)	2.12, ddd (13.6, 10.5, 8.1)	2.31, m	2.24, dd (14.1, 8.0)
10				1.74, t (10.5)	1.94, m	2.06, m
12				4.61, dd (10.3, 7.1)		
13a	2.47, m	2.32, m	2.43, m	2.07, m	2.34, m	2.32, m
13b	2.18, m	2.22, m	2.34, m	1.43, m	2.34, m	2.32, m
14	2.17, m	1.92, m	1.94, m	2.08, m	1.93, m	1.91, m
15	1.50, m	1.55, m	1.92, m	1.92, m	1.84, m	1.74, m
16a	4.79 d (2.1)	1.55, s	1.67, s	1.65, s	4.75, d (1.4)	5.15, d (2.5)
16b	4.73, d (2.1)				4.65, d (1.4)	4.92, d (2.5)
17a	4.97, d (3.5)	4.96, d (3.8)	1.57, s	1.56, s	3.93, dd (14.1, 6.5)	1.78, s
17b	4.87, d (3.5)	4.90, d (3.8)			3.75, dd (14.1, 5.1)	
18	0.95, s	0.89, s	0.82, s	0.77, s	1.01, s	0.91, s
19	0.94, d (6.6)	0.87, d (6.7)	1.12, d (6.3)	0.93, d (6.8)	1.07, d (6.6)	1.02, d (6.7)
20	0.83, d (6.6)	0.76, d (6.7)	0.94, d (6.3)	0.85, d (6.8)	0.92, d (6.6)	0.88, d (6.7)
-$COCH_3$				2.08, s		
2-OH						3.18, s
10-OH			3.59, s			
17-OH					3.41, dd (6.5, 5.1)	

[a]Recorded in CD_3OD; [b]Recorded in acetone-d_6.

C-7 (δ_C 149.8), and C-8 (δ_C 29.2); from H-6 (δ_H 2.70, dd, *J* = 15.4, 7.3 Hz) to C-1 (δ_C 39.6), C-8, and C-17 (δ_C 113.4); from H-8 (δ_H 1.62, dd, *J* = 9.1, 5.7 Hz) to C-10 (δ_C 35.1), C-11 (δ_C 52.4), and C-17; and from H_2-1 (δ_H 1.68, t, *J* = 13.9 Hz; 1.34, dd, *J* = 13.9, 4.6 Hz) to C-10 and C-11 collectively provided compelling evidence for the construction of a seven-membered ring B containing an exocyclic $\Delta^{7,17}$ double bond, fused to ring A through C-2 and C-6. Further HMBC correlations from both H_3-19 (δ_H 0.94, d, *J* = 6.6 Hz) and H_3-20 (δ_H 0.83, d, *J* = 6.6 Hz) to C-14 (δ_C 46.4) and C-15 (δ_C 28.4); from H_2-13 (δ_H 2.47, m; 2.18, m) to C-11 and C-12 (δ_C 224.4); and from both H-14 (δ_H 2.17, m) and H_3-18 (δ_H 0.95, s) to C-10, C-11, and C-12 allowed the establishment of a five-membered ring C bearing a methyl group at C-11, a ketone group at C-12, and an isopropyl group at C-14, which is fused to ring B through C-10 and C-11. Additionally, a characteristic aliphatic carbon resonance at δ_C 14.1 indicated the presence of a three-membered ring D, fused to the seven-membered ring B *via* C-8 and C-10. This deduction was confirmed by ^{1}H–^{1}H COSY correlation between H-8 and H_2-9, along with HMBC correlations from H_2-9 to C-7, C-10, and C-11. Ultimately, the planar structure of **1** was established as a previously unreported tetracyclic carbon skeleton consisting of a 5/7/5/3 ring system.

The relative configuration of **1** was elucidated by examining its ROESY spectrum (Fig. 3). Specifically, the observed ROESY correlations of H-2/H-9b, H-6/H-9b, H-2/H_3-18, H-8/H_3-14 indicated the α-orientations of H-2, H-6, and H_3-18, the β-orientations of H-8 and H-14, as well as the *R** configuration at C-10. Ultimately, the absolute configuration of **1** was determined to be 2*R*,6*R*,8*S*,10*R*,11*S*,14*S* by comparing its experimental ECD spectrum with the calculated spectrum (Fig. 4).

Hyperperin B (**2**) was isolated as a white amorphous powder. Its HR-ESI-MS data indicated that **2** shares the same molecular formula, $C_{20}H_{28}O$, as that of **1**. The ^{1}H and ^{13}C NMR data (Tables 1 and 2) demonstrated that **2** possesses an identical 5/7/5/3 tetracyclic carbon skeleton as **1**. The only difference was that **2** contains a tetrasubstituted double bond between C-2 and C-3, whereas **1** features a terminal double bond between C-3 and C-16. This deduction was corroborated by the HMBC correlations (Fig. 2) from H_2-1 (δ_H 2.45, d, *J* = 13.9 Hz; 1.79, d, *J* = 13.9 Hz), H_2-4 (δ_H 2.29, m; 2.21, m), and H-6 (δ_H 3.19, m) to C-2 (δ_C 135.9) and

Table 2 ^{13}C (125 MHz) NMR spectroscopic data of **1**–**12**.

Position	**1**[a]	**2**[b]	**3**[b]	**4**[a]	**5**[b]	**6**[b]	**7**[b]	**8**[b]	**9**[b]	**10**[b]	**11**[b]	**12**[b]
1	39.6	35.5	25.4	36.6	35.0	43.4	25.8	37.4	40.3	36.3	25.8	37.7
2	46.1	135.9	136.9	137.7	47.6	83.7	47.6	48.3	43.4	43.9	44.2	136.0
3	157.2	134.3	134.6	135.0	156.9	157.8	156.9	157.5	158.7	156.9	157.1	135.1
4	31.9	37.7	38.0	38.3	31.8	30.5	31.8	31.9	32.0	31.4	31.5	37.8
5	28.8	29.2	25.6	26.3	25.7	25.2	26.2	26.2	32.5	25.3	25.3	24.1
6	48.7	56.4	50.5	50.5	41.9	48.8	43.3	42.8	39.5	44.8	45.5	52.3
7	149.8	150.8	140.5	137.7	140.5	138.4	140.4	136.5	154.7	60.7	61.4	60.3
8	29.2	29.7	122.5	127.8	127.1	127.2	123.4	128.6	79.1	65.9	63.6	65.4
9	14.1	13.4	31.8	24.3	26.0	26.8	31.4	24.1	32.5	27.7	32.8	25.6
10	35.1	34.5	85.5	53.8	55.9	58.2	85.7	54.0	48.0	50.6	83.2	48.1
11	52.4	51.1	56.8	47.1	50.7	50.3	56.6	46.8	49.5	49.5	55.7	46.8
12	224.4	221.9	217.2	82.1	220.9	221.1	217.2	79.8	222.4	221.0	217.4	79.2
13	39.4	38.3	38.6	30.2	42.6	42.6	38.4	32.9	42.8	43.0	38.3	32.1
14	46.4	47.7	54.2	44.7	45.1	45.5	54.0	43.6	44.6	44.7	54.8	42.7
15	28.4	27.5	29.9	30.0	31.9	31.3	29.9	29.5	30.3	31.8	30.1	28.9
16	105.8	14.5	14.7	14.7	103.7	106.3	103.5	103.1	105.2	103.4	103.3	14.2
17	113.4	112.3	20.5	20.4	64.0	22.6	22.5	22.1	114.4	20.5	20.7	18.0
18	20.0	25.3	17.4	13.8	16.5	16.3	17.3	13.1	17.7	23.6	17.0	12.5
19	23.3	22.9	26.2	24.2	24.2	24.3	26.3	24.2	24.9	23.9	26.3	23.7
20	19.3	17.9	23.2	20.7	23.8	23.6	23.1	20.6	22.6	16.2	23.0	19.7
-$COCH_3$				173.1								
-$COCH_3$				21.0								

[a]Recorded in CD_3OD.; [b]Recorded in acetone-d_6.

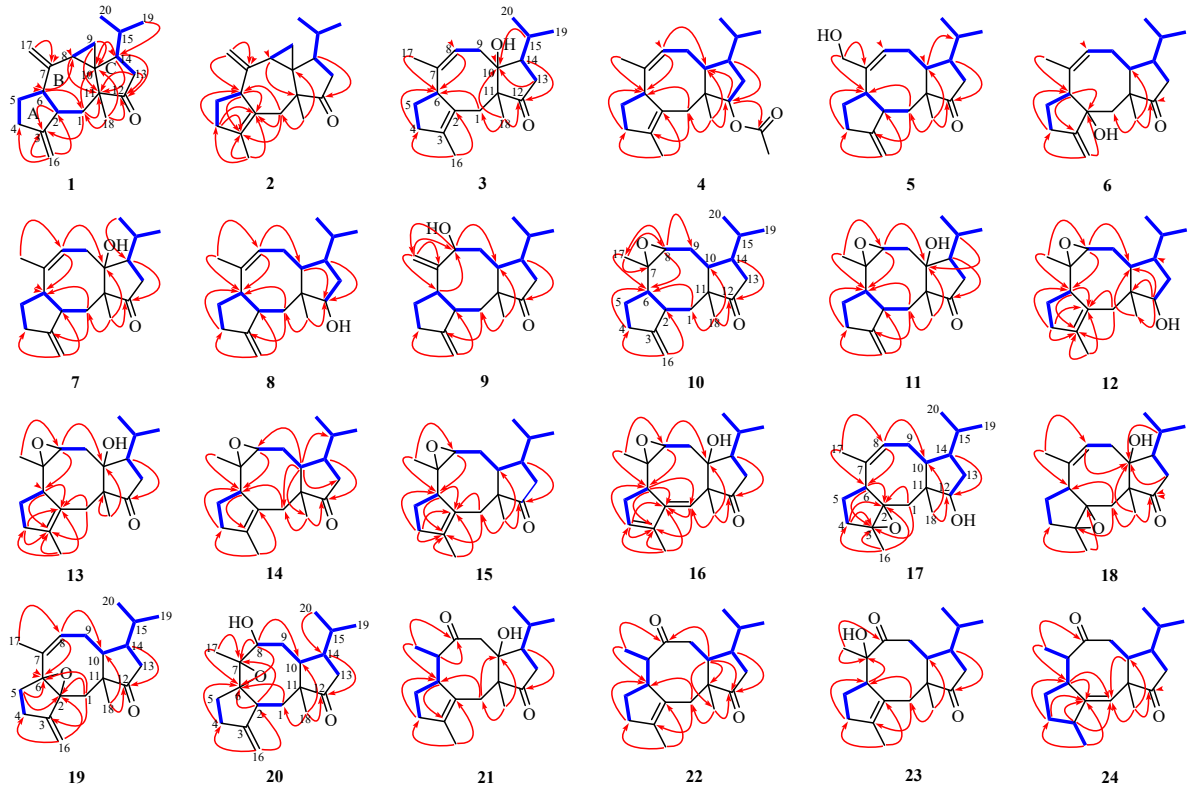


Fig. 2 Key ^1H–^1H COSY ( ) and HMBC ( ) correlations of **1**–**24**.

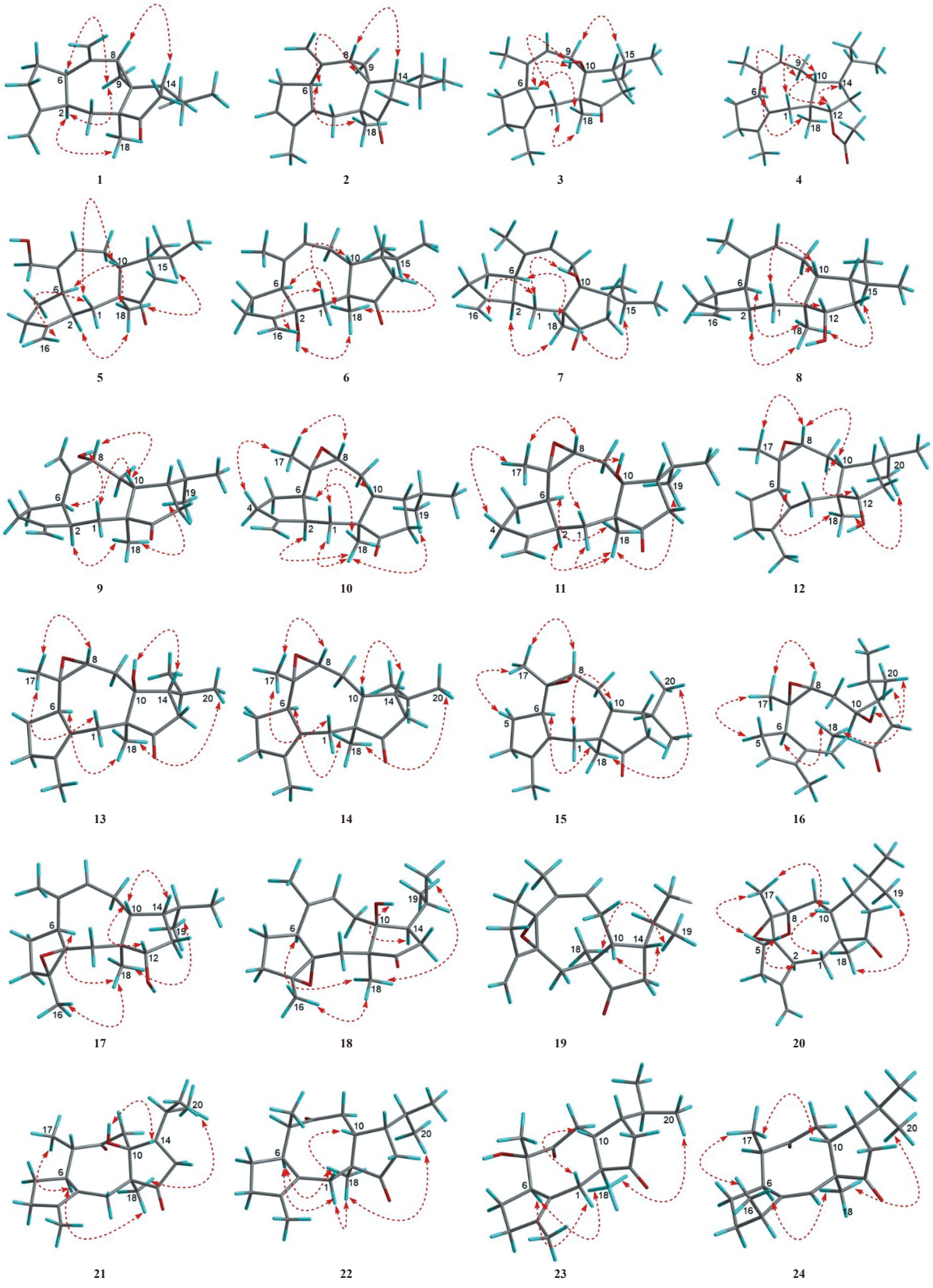


Fig. 3 Key ROESY ( ) correlations of **1**–**24**.

C-3 (δ_C 134.3), as well as from H_3-16 (δ_H 1.55, s) to C-2, C-3, and C-4 (δ_C 37.7). The relative configuration of **2** was determined based on ROESY data. The ROESY correlations (Fig. 3) involving H-6/H-9b, H-6/H_3-18, and H-8/H_3-14 indicated the α-orientations of H-6 and H_3-18, the β-orientations of H-8 and H_3-14, as well as the R^* configuration at C-10. Furthermore, the experimental ECD spectrum of **2** was in good agreement with the calculated spectrum (Fig. 4). Therefore, the absolute configuration of **2** was unambiguously established as 6*S*,8*S*,10*R*,11*S*,14*S*.

Hyperperin C (**3**) was obtained as a white amorphous powder with the molecular formula $C_{20}H_{30}O_2$, as determined by its HR-ESI-MS showing a peak at *m/z* 301.2172 $[M - H]^-$ (Calcd.

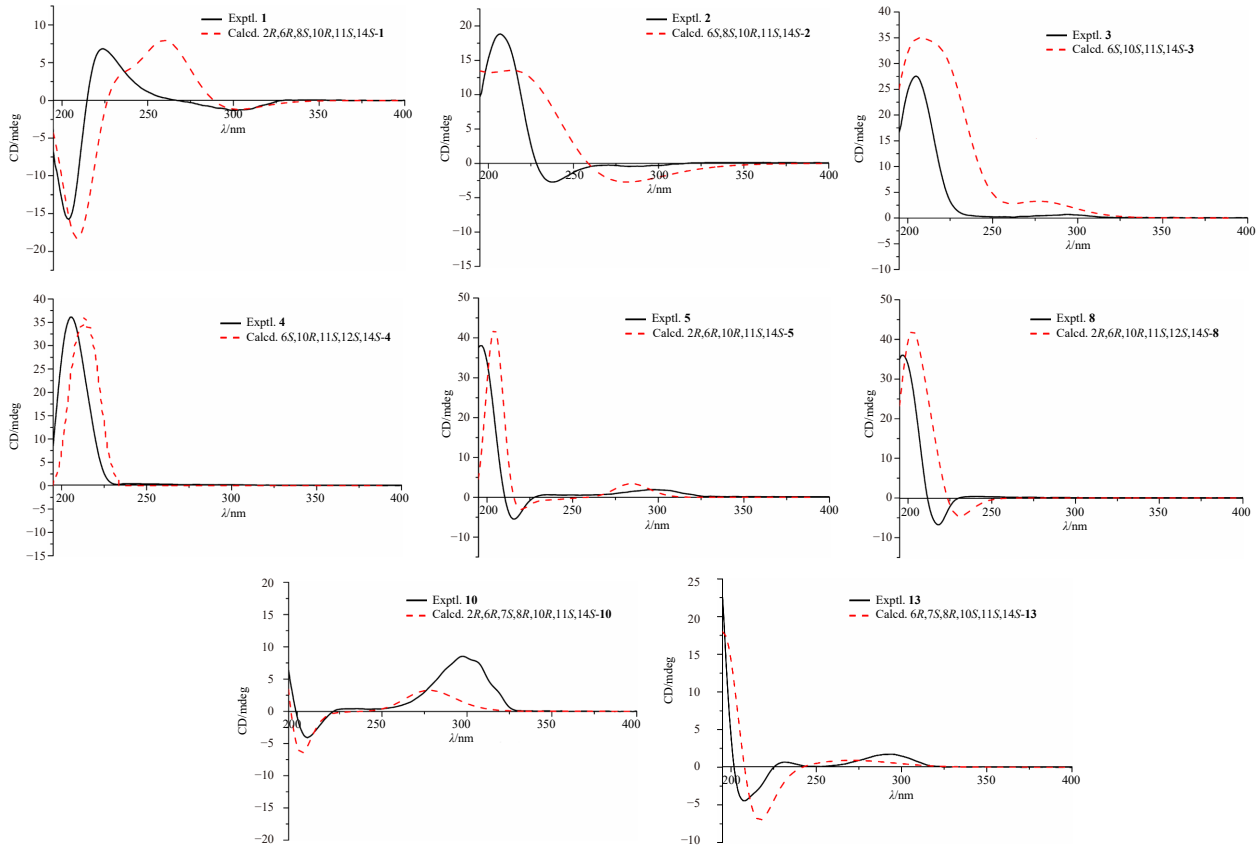


Fig. 4 Experimental and calculated ECD spectra of **1**–**5**, **8**, **10**, and **13**.

for 301.2173), suggesting six degrees of unsaturation. The IR spectrum exhibited characteristic absorption bands corresponding to hydroxyl (3489 cm^{-1}), ketone carbonyl (1719 cm^{-1}), and olefinic (1616 cm^{-1}) functionalities. Comprehensive analysis of the ^{1}H and ^{13}C NMR data (Tables 1 and 2) revealed that **3** contains 20 carbon atoms, comprising five methyl groups[δ_H 1.67 (3H, s, H_3-16), 1.57 (3H, s, H_3-17), 0.82 (3H, s, H_3-18), 1.12 (3H, d, J = 6.3 Hz, H_3-19), and 0.94 (3H, d, J = 6.3 Hz, H_3-20); δ_C 14.7 (C-16), 20.5 (C-17), 17.4 (C-18), 26.2 (C-19), and 23.2 (C-20)], five methylene groups, four methine groups including one olefinic methine [δ_H 5.44 (1H, dd, J = 9.7, 8.1 Hz, H-8); δ_C 122.5 (C-8)], and six quaternary carbons including three olefinic carbons [δ_C 136.9 (C-2), 134.6 (C-3), and 140.5 (C-7)], one oxygenated quaternary carbon [δ_C 85.5 (C-10)] and one ketone carbonyl carbon [δ_C 217.2 (C-12)]. The presence of two double bonds and one ketone carbonyl group accounts for three out of the six degrees of unsaturation, implying that **3** possesses a characteristic fusicoccane diterpenoid framework with a 5/8/5 tricyclic carbon skeleton. The 1D NMR data of **3** (Tables 1 and 2) were highly similar to those of hypoestin F [28], with the only difference being the substitution of a hydroxyl-bearing quaternary carbon at C-10 in **3**, in contrast to a methine group at the same position in hypoestin F. This structural difference was corroborated by the markedly deshielded resonance of C-10 ($\Delta\delta_C$ + 29.2), the HMBC correlations (Fig. 2) from H-8 (δ_H 5.44, dd, J = 9.7, 8.1 Hz), H_2-13 (δ_H 2.43, m; 2.34, m), H-15 (δ_H 1.92, m), and H_3-18 (δ_H 0.82, s) to C-10 (δ_C 85.5), as well as the molecular formula indicating one additional oxygen atom. ROESY cross-peaks (Fig. 3) of H-6/H-9a, H-6/H_3-18, H-9b/H-15, 10-OH/H-1a, and H-1b/ H_3-18 demonstrated that H-6 and H_3-18 are α-oriented, while 10-OH and H-14 are β-oriented. The experimental ECD spectrum of **3** aligned well with the calculated spectrum (Fig. 4). Consequently, the absolute configuration of **3** was conclusively assigned as 6*S*,10*S*,11*S*,14*S*.

Hyperperin D (**4**) was assigned the molecular formula $C_{22}H_{34}O_2$, consistent with its HR-ESI-MS data, which showed a peak at *m/z* 353.2450 $[M + Na]^+$, Calcd. for 353.2451), corresponding to six degrees of unsaturation. A comprehensive comparison of the ^{1}H and ^{13}C NMR data of **4** (Tables 1 and 2) with those of hypoestin F demonstrated a close structural similarity between the two molecules [28]. The key structural distinction was the presence of an acetoxy group [δ_H 2.08 (3H, s), δ_C 21.0, 173.1] at C-12 in **4**, rather than the ketone carbonyl group at C-12 in hypoestin F. This assignment was confirmed by key HMBC correlation (Fig. 2) from H-12 (δ_H 4. 61, dd, J = 10.3, 7.1 Hz) to the acetyl carbonyl carbon, along with ^{1}H-^{1}H COSY correlations of H-12/H_2-13/H-14. The α-orientation of the acetoxy group at C-12 was deduced from ROESY cross-peaks (Fig. 3) of H-12 with H-10 and H-14. Further analysis of the ROESY data confirmed that the relative configurations of the remaining stereogenic centers were identical to those of hypoestin F. Finally, the absolute configuration of **4** was determined as 6*S*,10*R*,11*S*,12*S*,14*S* by comparison of its experimental ECD spectrum with the calculated spectrum (Fig. 4).

Hyperperins E–G (**5**–**7**) were assigned to have the same molecular formula, $C_{20}H_{30}O_2$, based on their HR-ESI-MS and ^{13}C NMR data. Examination of the 1D NMR data for **5**–**7** (Tables 1–3) revealed that they possess a fusicoccane diterpenoid scaffold with a 5/8/5 tricyclic ring system, identical to that found in fusicocc-4(16),8(9)-dien-14-one (**25**) [25]. The closely comparable 1D NMR data of **5** and **25** indicated that these molecules are structural analogues, with the notable difference being the substitution at C-7, where **5** features a hydroxymethyl group in place of the methyl group present in **25**. This substitution was corroborated by a pronounced downfield-shifted resonance of C-17 ($\Delta\delta_C$ + 42.1), further supported by HMBC correlations (Fig. 2) from H_2-17 (δ_H 3.93, dd, J = 14.1, 6.5 Hz; 3.75, dd, J = 14.1, 5.1 Hz) to C-6 (δ_C 41.9), C-7 (δ_C 140.5), and C-8 (δ_C 127.1). Comparison of the ^{1}H and ^{13}C NMR data for **6** (Tables 1 and 2) with those of **25** revealed that these two compounds are structurally closely rela-

ted [25], with the key distinction being the presence of a hydroxyl group at C-2 in **6**. The pronounced downfield shift of the C-2 resonance ($\Delta\delta_C$ + 36.0) and the characteristic hydroxyl absorption band at 3496 cm^{-1} in the IR spectrum verified the attachment of the hydroxyl group at C-2 in **6**. Similarly, comparing the 1D NMR data of **7** (Tables 2 and 3) with those of **25** demonstrated that **7** shares a closely related structure with **25**. The main difference lay in the presence of a hydroxyl group at C-10 in **7**. This deduction was confirmed by the pronounced downfield shift of the C-10 resonance ($\Delta\delta_C$ + 29.1), the characteristic hydroxyl absorption band at 3504 cm^{-1} in the IR spectrum, and the detection of an additional oxygen atom in the molecular formula of **7** compared to **25**. ROESY cross-peaks (Fig. 3) of H_3-18 with H-2, H-6, and H-15, as well as H-1b with H-10 and H-16b, validated that H-2, H-6, and H_3-18 adopt α-orientations, whereas H-10 and H-14 exhibit β-orientations in **5**. Based on ROESY analysis (Fig. 3), the relative configurations of **6** and **7** were assigned to be the same as that of **5**. The calculated ECD spectrum of **5** showed good agreement with the experimental spectrum (Fig. 4), allowing for the definitive determination of its absolute configuration as 2*R*,6*R*,10*R*,11*S*,14*S*. Furthermore, the experimental ECD spectra of **6** and **7** (Fig. 5) matched that of **5**, leading to the assignment of their absolute configurations as 2*S*,6*S*,10*R*,11*S*,14*S* and 2*R*,6*R*,10*S*,11*S*,14*S*, respectively.

Hyperperin H (**8**), obtained as a white amorphous powder, has a molecular formula of $C_{20}H_{32}O$, as deduced from its HR-ESI-MS ion peak at *m/z* 311.2344 $[M + Na]^+$ (Calcd. for 311.2345), corresponding to five degrees of unsaturation. A comparison of the 1D NMR data of **8** (Tables 2 and 3) with those of **25** revealed notable similarities, indicating that these two compounds are structural analogs [25]. The primary distinction was that the carbonyl group at C-12 in **25** was replaced by a hydroxyl group at the same position in **8**. This deduction was supported by HMBC correlations (Fig. 2) from H-10 (δ_H 1.56, t, *J* = 10.9 Hz) and H_3-18 (δ_H 0.86, s) to C-12 (δ_C 79.8), as well as key $^1H–^1H$ COSY correlations (Fig. 2) of H-12/H_2-13/H-14. The α-orientation of the hydroxyl group at C-12 was inferred from the ROESY cross-peaks (Fig. 3) between H-12/H-10 and 12-OH/H_3-20. The relative configurations of the remaining stereogenic centers are consistent with those of **25**, as confirmed by ROESY analysis. To establish the absolute configuration of **8**, ECD calculations were carried out. As depicted in Fig. 4, the experimental ECD spectrum of **8** closely matched the calculated spectrum for the 2*R*,6*R*,10*R*,11*S*,12*S*,14*S* configuration. Thus, the absolute configuration of **8** was unambiguously assigned as 2*R*,6*R*,10*R*,11*S*,12*S*,14*S*.

Hyperperin I (**9**) was isolated as colorless crystals. Its molecular formula, $C_{20}H_{30}O_2$, corresponding to six degrees of unsaturation, was determined by the HR-ESI-MS ion peak at *m/z* 325.2136 $[M + Na]^+$ (Calcd. for $C_{20}H_{30}O_2Na$, 325.2138). The IR spectrum showed characteristic absorption bands for hydroxyl (3416 cm^{-1}), ketone carbonyl (1719 cm^{-1}), and olefinic (1645 cm^{-1}) functionalities. The 1D NMR data of **9** (Tables 2 and 3) exhibited marked similarities to those of **25** [25], with key distinctions including a terminal double bond at C-7/C-17 in **9**, replacing the trisubstituted double bond at C-7/C-8 found in **25**, as well as the presence of a hydroxyl group at C-8 in **9**. Diagnostic HMBC correlations (Fig. 2) from H_2-17 (δ_H 4.95, br s and 4.70, br s) to C-6 (δ_C 39.5), C-7 (δ_C 154.7), and C-8 (δ_C 79.1) corroborated the existence of the terminal double bond between C-7 and C-17. The 8-OH group was further confirmed by HMBC correlations of H-6 (δ_H 2.99, m) and H_2-17 to C-8, and of H-8 (δ_H 4.09, m) to C-10 (δ_C 48.0), coupled with key $^1H–^1H$ COSY correlations (Fig. 2) of H-8/H_2-9/H-10. The α-orientation of the hydroxyl group at C-8 was inferred from ROESY cross-peaks (Fig. 3) of H-8/H-10 and 8-OH/H-6. The relative configurations of H-2, H-6, H-10, H-11, and H-14 were identical to those of **25**, as evidenced by their similar ROESY correlations. Finally, a successful single-crystal X-ray diffraction analysis of **9** not only corroborated the proposed structural assignments but also unambiguously established its absolute configuration as 2*R*,6*R*,8*R*,10*R*,11*S*,14*S* with a Flack parameter of 0.02(7) (Fig. 6).

Hyperperin J (**10**) has a molecular formula of $C_{20}H_{30}O_2$, containing one more oxygen atom than **25**, as determined by its HR-ESI-MS and ^{13}C NMR data. The ^1H and ^{13}C NMR data of **10** (Tables 2 and 3) closely resembled those of **25** [25], except for the presence of a trisubstituted 7,8-epoxide moiety in **10** instead of the trisubstituted double bond between C-7 and C-8 in **25**. This deduction was corroborated by the upfield shifts in the C-7 ($\Delta\delta_C$ − 76.4) and C-8 resonances ($\Delta\delta_C$ − 62.0), along with diagnostic HMBC correlations (Fig. 2) from H-8 (δ_H 2.70, dd, *J* = 9.7, 5.2 Hz) to C-6 (δ_C 44.8) and C-17 (δ_C 20.5); from H_3-17 (δ_H 0.99, s) to C-6, and C-7 (δ_C 60.7); and key $^1H–^1H$ COSY correlations (Fig. 2) of H-8/H_2-9/H-10. Additionally, ROESY correlations (Fig. 3) of H-1b with H-10, H_3-17 with H-8 and H-4a, as well as H_3-18 with H-1a, H-2, and H_3-19, indicated the α-orientations of H-2, H-6, and H_3-18, while the β-orientations of H-10, H-14, and H_3-17. As illustrated in Fig. 4, the calculated ECD spectrum matched well with the experimental data. Collectively, these findings established the absolute configuration of **10** as 2*R*,6*R*,7*S*,8*R*,10*R*,11*S*,14*S*.

Hyperperin K (**11**) was assigned the molecular formula $C_{20}H_{30}O_3$ based on the HR-ESI-MS ion at *m/z* 341.2089 $[M + Na]^+$ (Calcd. for $C_{20}H_{30}O_3Na$, 341.2087). Interpretation of the IR spectrum of **11** revealed the presence of hydroxyl (3479 cm^{-1}), carbonyl (1731 cm^{-1}), and olefinic (1653 cm^{-1}) groups. The nearly identical 1D NMR data of **11** (Tables 2 and 3) and **10** indicated that these compounds are structural analogs, differing only by the presence of a hydroxyl group at C-10 in **11** instead of a methine group at the same position in **10**. The deshielded resonance of C-10 ($\Delta\delta_C$ + 32.6), along with key HMBC correlations (Fig. 2) from H-8 (δ_H 2.96, dd, *J* = 9.4, 5.4 Hz), H-15 (δ_H 1.89, m), and H_3-18 (δ_H 0.94, s) to C-10 (δ_C 83.2), confirmed that the assignment of the hydroxyl group at C-10. The β-orientation of this hydroxyl group was inferred from ROESY cross-peaks (Fig. 3) of 10-OH/H-1b and H-1a/H_3-18. The relative configurations of H-2, H-6, H-14, H_3-17, and H_3-18 in **11** were identical to those of **10**, as evidenced by their comparable ROESY correlations. Furthermore, the experimental ECD spectrum (Fig. 5) of **11** closely matched that of **10**, allowing the absolute configuration of **11** to be assigned as 2*R*,6*R*,7*S*,8*R*,10*S*,11*S*,14*S*.

Hyperperin L (**12**) was assigned the molecular formula $C_{20}H_{32}O_2$ based on HR-ESI-MS and ^{13}C NMR data. The 1D NMR data of **12** (Tables 2 and 3) closely mirrored those of **10**, indicating that these molecules are structural analogs. The primary discrepancy lied in the replacement of the ketone carbonyl group at C-12 in **10** with a hydroxyl-substituted methine in **12**. This deduction was clarified by $^1H–^1H$ COSY cross-peaks (Fig. 2) for the spin system H-12/H_2-13/H-14, the HMBC correlations from H-12 (δ_H 3.59, dt, *J* = 10.8, 6.8 Hz) to C-10 (δ_C 48.1), C-11 (δ_C 46.8), C-14 (δ_C 42.7), and C-18 (δ_C 12.5), as well as the upfield shift of the C-12 resonance ($\Delta\delta_C$ − 141.8). Furthermore, compound **12** features a tetrasubstituted double bond at C-2/C-3, in contrast to the terminal double bond at C-3/C-16 observed in **10**. This deduction was confirmed by the HMBC correlations (Fig. 2) from H_2-1 (δ_H 2.93, d, *J* = 14.5 Hz; 1.44, d, *J* = 14.5 Hz), H_2-4 (δ_H 2.27, m), H-6 (δ_H 2.49, m), and H_3-16 (δ_H 1.64, s) to C-2 (δ_C 136.0) and C-3 (δ_C 135.1). The downfield shift of the C-2 ($\Delta\delta_C$ + 92.1), along with the upfield shifts of C-3 ($\Delta\delta_C$ − 21.8) and C-16 ($\Delta\delta_C$ − 89.2), further consolidated this structural assignment. The ROESY correlations (Fig. 3) involving H-6/H_3-18, H-8/H-10, H-10/H-12, H-8/H_3-17, and H_3-18/H_3-20 indicated that H-6, H_3-18, and 12-OH are α-oriented, while H-8, H-10, H-12, H-14, and H_3-17 are β-oriented. Ultimately, single crystals of **12** suitable for X-ray diffraction analysis were successfully obtained through crystallization from MeOH. This process not only validated the relative configuration

Table 3 ^{1}H (500 MHz) NMR spectroscopic data of **7**–**12** in acetone-d_6 (J in Hz).

Position	7	8	9	10	11	12
1a	2.04, m	2.11, dd (13.7, 4.3)	1.90, dd (14.0, 3.8)	2.48, m	2.20, dd (14.9, 4.1)	2.93, d (14.5)
1b	1.35, dd (14.8, 12.0)	0.84, m	1.06, dd (14.0, 11.0)	0.95, m	1.69, dd (14.9, 12.3)	1.44, d (14.5)
2	2.53, m	2.42, m	2.69, m	2.50, m	2.48, m	
4a	2.51, m	2.50, m	1.94, m	2.51, m	2.51, m	2.27, m
4b	2.42, m	2.38, m	1.67, m	2.43, m	2.44, m	2.27, m
5a	1.88, m	1.84, m	2.42, m	1.91, m	1.91, m	1.87, m
5b	1.88, m	1.84, m	2.42, m	1.91, m	1.91, m	1.77, m
6	3.21, t (5.5)	3.26, m	2.99, m	2.08, m	2.05, m	2.49, m
8	5.39, t (8.0)	5.42, t, 8.1	4.09, m	2.70, dd (9.7, 5.2)	2.96, dd (9.4, 5.4)	2.71, dd (9.7, 5.1)
9a	2.74, dd (13.6, 8.0)	2.24, m	2.19, m	2.37, dd (13.8, 5.2)	2.63, dd (14.1, 5.4)	2.17, dd (13.9, 5.1)
9b	2.43, dd (11.0, 8.0)	2.00, dd (13.5, 8.1)	1.84, m	1.63, ddd (13.8, 11.0, 9.7)	1.84, dd (14.1, 9.4)	1.40, m
10		1.56, t (10.9)	1.86, m	2.21, dd (11.0, 7.2)		1.85, m
12		3.50, ddd (10.5, 7.2, 5.9)				3.59, dt (10.8, 6.8)
13a	2.40, m	1.83, m	2.28, m	2.41, m	2.50, m	1.83, m
13b	2.37, m	1.42, ddd (12.8, 10.5, 8.7)	2.28, m	2.41, m	2.40, m	1.42, m
14	1.93, m	1.94, m	1.98, m	2.00, m	2.00, m	2.07, m
15	1.96, m	1.86, m	1.72, m	1.79, m	1.89, m	1.88, m
16a	4.76, d (4.5)	4.71, d (1.9)	4.87, d (2.0)	4.81, d (2.2)	4.85, d (2.5)	1.64, s
16b	4.76, d (4.5)	4.66, d (1.9)	4.70, d (2.0)	4.76, d (2.2)	4.82, d (2.5)	
17a	1.58, s	1.52, s	4.95, br s	0.99, s	1.00, s	1.02, s
17b			4.70, br s			
18	1.04, s	0.86, s	0.96, s	0.93, s	0.94, s	0.54, s
19	1.13, d (6.4)	0.88, d (6.7)	1.04, d (6.6)	1.04, d (6.7)	1.13, d (6.7)	0.87, d (6.8)
20	0.96, d (6.4)	0.83, d (6.7)	0.87, d (6.6)	0.92, d (6.7)	0.96, d (6.7)	0.77, d (6.8)
8-OH			3.80, d (3.3)			
10-OH					3.98, s	
12-OH		3.63, d (5.8)				3.79, d (6.8)

but also definitively determined the absolute configuration as 6*R*,7*S*,8*R*,10*R*,11*S*,12*S*,14*S* [Flack parameter = 0.17(4)] (Fig. 6).

Hyperperin M (**13**) was determined to possess the same molecular of, $C_{20}H_{30}O_3$, as **11**, based on the sodium adduct ion signal at *m/z* 341.2088 $[M + Na]^+$ observed in the HR-ESI-MS spectrum, compatible with six degrees of unsaturation. The IR spectrum showed absorptions at 3493, 1744, and 1621 cm^{-1}, corresponding to hydroxyl, carbonyl, and olefinic functional groups, respectively. A comparative analysis of the ^{1}H and ^{13}C NMR spectroscopic data for **13** (Tables 4 and 5) and **11** demonstrated that these two molecules share closely related structures. The primary structural difference included that **13** has a tetrasubstituted double bond between C-2 and C-3, whereas **11** features a terminal double bond between C-3 and C-16. This deduction was assigned by HMBC correlations (Fig. 2) from H_3-16 (δ_H 1.69, s) to C-2 (δ_C 135.6), C-3 (δ_C 133.5), and C-4 (δ_C 37.1), as well as from H-1a (δ_H 2.75, d, J = 15.2 Hz), H-1b (δ_H 2.23, d, J = 15.2 Hz), H_2-4 (δ_H 2.31, m), and H-6 (δ_H 2.51, m) to C-2 and C-3. ROESY cross-peaks (Fig. 3) involving H-6/H_3-18, H_3-17/H-1b, H_3-17/H-8, 10-OH/H-14, and H_3-18/H_3-20 revealed the α-orientations of H-6 and H_3-18, as well as the β-orientations of H-8, H-14, H_3-17, and 10-OH. Additionally, single-crystal X-ray diffraction analysis of **13** was performed, confirming its planar structure and relative configuration (Fig. 6). Further ECD calculations (Fig. 4) showed that the experimental ECD spectrum of **13** closely matched the calculated spectrum for the 6*R*,7*S*,8*R*,10*S*,11*S*,14*S* configuration, definitively assigning its absolute configuration as 6*R*,7*S*,8*R*,10*S*,11*S*,14*S*.

Hyperperin N (**14**) has the molecular formula $C_{20}H_{30}O_2$, containing one fewer oxygen atom than **13**, as determined by (+)-HR-ESI-MS and ^{13}C NMR data. The 1D NMR data of **14** (Tables 4 and 5) mirrored those of **13**, with the only difference being the absence of a hydroxyl group at C-10 (δ_C 50.7) in **14**. This deduction was corroborated by HMBC correlations (Fig. 2) from H-10 (δ_H 2.27, m) to C-1 (δ_C 35.7), C-8 (δ_C 64.9), C-13 (δ_C 43.2), and C-18 (δ_C 16.5), as well as key ^{1}H–^{1}H COSY correlations of H-8/H_2-9/H-10/H-14. The relative configuration of **14** was assigned as identical to that of **13** based on ROESY data (Fig. 3). As shown in Fig. 5, the ECD spectrum of **14** was highly superimposable on that of **13**, thus confirming its absolute configuration as 6*R*,7*S*,8*R*,10*R*,11*S*,14*S*.

Hyperperin O (**15**) shares the same molecular formula, $C_{20}H_{30}O_2$, as **10**, based on HR-ESI-MS analysis. The 1D NMR data of **15** (Tables 4 and 5) suggested that its structure is comparable

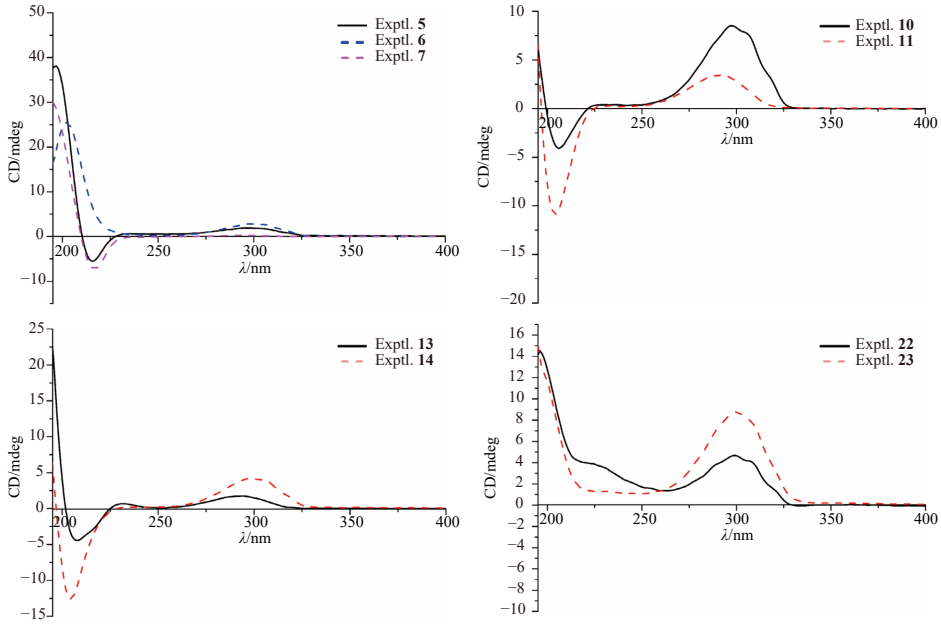


Fig. 5 Experimental ECD spectra of **5**–**7**, **10**, **11**, **13**, **14**, **22**, and **23**.

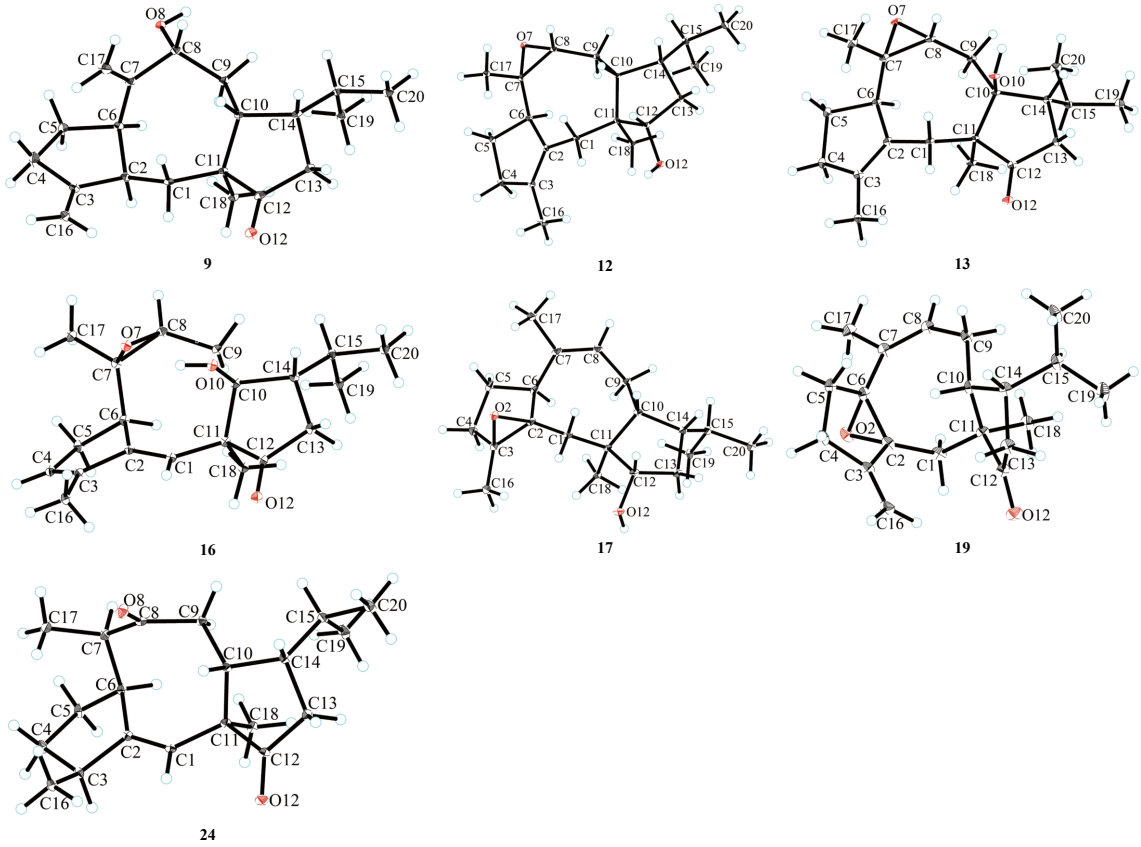


Fig. 6 X-ray crystal structures of **9**, **12**, **13**, **16**, **17**, **19**, and **24**.

to that of **10**, with the sole difference being that **15** bears a tetrasubstituted double bond at C-2 and C-3, instead of the terminal double bond between C-3 and C-16 in **10**. This deduction was confirmed by HMBC correlations (Fig. 2) from H_2-1 (δ_H 2.59, d, J = 14.1 Hz; 1.74, d, J = 14.1 Hz), H_2-4 (δ_H 2.35, m; 2.05, m), H-6 (δ_H 2.88, m), and H_3-16 (δ_H 1.45, s) to C-2 (δ_C 138.7) and C-3 (δ_C 133.7). Moreover, the downfield shift observed for the C-2 carbon signal ($\Delta\delta_C$ + 94.8) and the upfield shift of the C-16 carbon signal ($\Delta\delta_C$ -88) further corroborated this structural assignment. ROESY cross-peaks (Fig. 3) involving H-6/H_3-18, H-10/H-1b, H_3-17/H-8, H_3-17/H-5b, and H_3-18/H_3-20 revealed the α-orientations of H-6, H-8, H_3-17, and H_3-18, as well as the β-orientations of H-10 and H-14. Finally, a direct comparison between the calculated and experimental ECD spectra of **15** (Fig. 7) unambiguously confirmed its absolute configuration as 6*R*,7*R*,8*S*,10*R*,11*S*,14*S*.

Hyperperin P (**16**) was assigned the molecular formula $C_{20}H_{28}O_3$, which was deduced from its HR-ESI-MS sodium adduct ion peak at *m/z* 339.1930 $[M + Na]^+$ (Calcd. 339.1931) and the ^{13}C

NMR data. A comparison of the 1D NMR data of **16** (Tables 4 and 5) with those of **15** revealed striking similarities, indicating that those two compounds are structural congeners. Specifically, the tetrasubstituted double bond located at C-2 and C-3 in **15** was replaced by conjugated double bonds at C-1/C-2 and C-3/C-4 in **16**. This deduction was corroborated by HMBC correlations (Fig. 2) from H-1 (δ_H 5.62, d, J = 1.9 Hz) to C-2 (δ_C 142.2) and C-3 (δ_C 149.6), from H-4 (δ_H 5.79, br s) to C-2 and C-3, from H-6 (δ_H 3.39, td, J = 5.1, 2.1 Hz) to C-1 (δ_C 119.6), C-2, and C-3, from H_3-16 (δ_H 1.73, s) to C-2, C-3, and C-4 (δ_C 131.1). Additionally, the presence of a hydroxyl group at C-10 (δ_C 85.2) in **16** instead of the methine group at C-10 in **15** was confirmed by the significant downfield shift observed for C-10 ($\Delta\delta_C$ + 44.5). Based on ROESY analysis (Fig. 3), the relative configurations at the stereocenters C-6, C-7, C-8, C-10, C-11, and C-14 of **16** were consistent with those of **15**. Ultimately, successful X-ray diffraction analysis (Fig. 6) definitively established the absolute configuration of **16** as 6*R*, 7*R*, 8*S*, 10*S*, 11*S*,14*S*, with a Flack parameter of 0.01(6).

Hyperperin Q (**17**) was assigned the molecular formula $C_{20}H_{32}O_2$ based on its HR-ESI-MS and ^{13}C NMR data. Interpretation of the IR spectrum of **17** indicated the presence of typical hydroxyl (3399 cm^{-1}) and olefinic (1631 cm^{-1}) groups. The 1D NMR spectroscopic data of **17** (Tables 4 and 5) were similar to those of **8**, with the exception of the lack of the terminal double bond at C-3 and C-16 in **8** and the appearance of a 2,3-epoxide unit in **17**. This assignment was supported by the chemical shifts of C-2 at δ_C 72.7 and C-3 at δ_C 66.5, as well as key HMBC correlations (Fig. 2) from H-1a (δ_H 1.75, d, J = 14.4 Hz), H-1b (δ_H 1.43, d, J = 14.4 Hz), H-4a (δ_H 1.86, m), H-4b (δ_H 1.60, m), H-6 (δ_H 3.08, dd, J = 10.8, 7.3 Hz), and H_3-16 (δ_H 1.31, s) to C-2 and C-3. In the ROESY spectrum (Fig. 3), cross-peaks were detected of H-6/H_3-18, H_3-16/H_3-18, H_3-18/H_3-19, of H-10/H-12, and of H-10/H-14, suggesting that the α-orientations of H-6, H-16, and H_3-18, as well as the β-orientations of H-10, H-12, and H-14. However, the relative configurations at C-2 and C-3 couldn't be determined through ROESY analysis. Luckily, single-crystal X-ray crystallography using Cu Kα radiation [Flack parameter = 0.12(6)] definitively determined both the structure and absolute configurations of **17** as 2*R*, 3*S*, 6*S*, 10*R*, 11*S*, 12*S*,14*S* (Fig. 6).

Hyperperin R (**18**), a white amorphous powder, has a molecular formula of $C_{20}H_{30}O_3$, as established by the HR-ESI-MS ion at *m/z* 341.2090 $[M + Na]^+$ (Calcd. for $C_{20}H_{30}O_3Na$, 341.2087). Its IR spectrum displayed absorption bands for hydroxyl (3441 cm^{-1}), ketone carbonyl (1734 cm^{-1}), and double bond (1629 cm^{-1}) functional groups. The ^1H and ^{13}C NMR data of **18** (Tables 4 and 5) were similar to those of **17**, except for the presence of an additional hydroxyl group at C-10 in **18**, and the replacement of the hydroxyl group at C-12 in **17** by a ketone carbonyl group in **18**. HMBC correlations (Fig. 2) from H_2-13 (δ_H 2.44, m; 2.39, m), H-14 (δ_H 1.95, m), and H_3-18 (δ_H 1.00, s) to C-12 (δ_C 216.5) verified the presence of the ketone carbonyl group at C-12. The presence of the 10-OH group was confirmed by HMBC correlations from H-8 (δ_H 5.51, t, J = 7.9 Hz), H_2-13 (δ_H 2.44, m; 2.39, m), H-15 (δ_H 1.95, m), and H_3-18 (δ_H 1.00, s) to C-10 (δ_C 85.2), together with the

Table 4 ^1H NMR spectroscopic data of **13**–**18** in acetone-d_6 (J in Hz).

Position	13[a]	14[a]	15[a]	16[a]	17[a]	18[b]
1a	2.75, d (15.2)	3.03, d (14.8)	2.59, d (14.1)	5.62, d, 1.9	1.75, d (14.4)	2.07, d (14.5)
1b	2.23, d (15.2)	1.50, d (14.8)	1.74, d (14.1)		1.43, d (14.4)	1.64, d (14.5)
4a	2.31, m	2.31, m	2.35, m	5.79, br s	1.86, m	1.89, dd (13.5, 7.6)
4b	2.31, m	2.31, m	2.05, m		1.60, m	1.61, m
5a	1.88, m	1.88, m	2.12, m	2.59, m	1.42, m	1.45, m
5b	1.81, m	1.79, m	1.99, m	2.59, m	1.31, m	1.32, m
6	2.51, m	2.51, m	2.88, m	3.39, td (5.1, 2.1)	3.08, dd (10.8, 7.3)	3.03, dd (10.6, 7.4)
8	3.04, dd (9.2, 5.3)	2.79, dd (9.5, 5.1)	3.01, m	3.05, dd (8.9, 2.8)	5.59, t (8.0)	5.51, t (7.9)
9a	2.65, dd (14.2, 5.3)	2.39, m	2.25, dd (17.8, 2.5)	2.64, dd (15.2, 2.8)	2.29, dd (11.8, 8.0)	2.84, dd (14.0, 7.9)
9b	1.86, m	1.65, m	2.18, dd (17.8, 8.2)	2.32, dd (15.2, 8.9)	2.10, dd (11.8, 8.0)	2.49, dd (14.0, 7.9)
10		2.27, m	2.33, m		1.67, m	
12					3.46, ddd (10.8, 7.1, 6.1)	
13a	2.50, m	2.40, m	2.34, m	2.51, dd (18.9, 3.2)	1.81, m	2.44, m
13b	2.37, m	2.40, m	2.34, m	2.40, m	1.41, m	2.39, m
14	1.99, m	1.99, m	1.88, m	2.06, m	2.00, m	1.95, m
15	1.85, m	1.73, m	1.72, m	2.06, m	1.90, m	1.95, m
16	1.69, s	1.68, s	1.45, s	1.73, s	1.31, s	1.34, s
17	1.02, s	1.02, s	1.28, s	1.30, s	1.63, s	1.68, s
18	0.71, s	0.68, s	1.03, s	1.25, s	0.83, s	1.00, s
19	1.11, d (6.7)	1.03, d (6.5)	1.00, d (6.7)	1.17, d (6.2)	0.87, d (6.7)	1.13, d (6.0)
20	0.93, d (6.7)	0.91, d (6.5)	0.82, d (6.7)	0.98, d (6.2)	0.82, d (6.7)	0.95, d (6.0)
10-OH	4.05, s			3.99, s		3.71, s
12-OH					3.74, d (6.1)	

[a]Recorded at 500 MHz; [b]Recorded at 600 MHz.

Table 5 ^{13}C NMR spectroscopic data of **13**–**24** in acetone-d_6.

Position	**13**[a]	**14**[a]	**15**[a]	**16**[a]	**17**[a]	**18**[b]	**19**[a]	**20**[a]	**21**[a]	**22**[b]	**23**[a]	**24**[a]
1	24.7	35.7	38.1	119.6	39.2	27.5	38.7	48.7	26.5	35.9	36.6	129.8
2	135.6	137.7	138.7	142.2	72.7	72.9	72.0	45.7	138.4	138.6	140.7	152.0
3	133.5	133.3	133.7	149.6	66.5	66.3	150.8	156.8	134.6	133.4	132.4	42.3
4	37.1	37.8	37.6	131.1	32.9	32.7	28.7	27.9	36.5	37.7	38.0	33.4
5	23.0	24.1	28.8	35.2	21.4	21.3	30.3	30.6	29.1	25.9	25.8	32.2
6	51.8	51.9	54.3	42.8	43.5	44.0	74.4	74.6	53.2	54.3	63.6	43.8
7	60.1	60.2	66.9	63.8	136.3	139.3	132.4	65.4	55.3	49.8	81.6	54.1
8	61.9	64.9	68.3	62.8	127.9	122.9	125.8	71.8	216.8	214.9	216.3	214.5
9	32.7	28.1	43.8	33.5	24.3	32.2	29.8	31.1	43.3	42.8	39.7	41.6
10	82.5	50.7	40.7	85.2	53.8	85.2	43.4	46.1	82.9	46.2	44.3	46.9
11	55.3	50.2	49.3	57.8	45.3	54.9	50.6	48.9	56.5	49.9	50.3	51.8
12	216.3	221.1	223.0	216.8	79.4	216.5	223.7	223.4	215.4	221.3	221.6	220.4
13	37.5	43.2	28.4	37.3	32.3	38.3	42.9	39.7	38.2	42.6	42.3	41.4
14	54.2	45.1	45.5	53.7	43.4	54.4	44.5	44.9	54.9	45.2	44.5	45.1
15	29.2	31.6	30.4	28.4	29.0	29.9	28.3	26.9	29.5	30.2	29.7	30.3
16	13.3	14.2	15.4	13.3	16.1	16.2	111.9	106.5	14.6	14.5	14.7	21.7
17	17.0	17.9	28.9	25.0	21.1	21.4	22.9	17.9	17.2	12.2	19.4	12.6
18	16.3	16.5	21.8	19.4	12.7	17.3	22.8	18.2	18.4	20.2	20.4	18.3
19	25.2	23.8	24.7	26.1	23.9	26.2	26.3	25.0	25.7	24.2	24.5	24.7
20	22.3	23.6	22.7	21.8	20.2	23.1	22.6	19.6	22.8	23.1	22.9	22.8

[a]Recorded at 125 MHz, [b]Recorded at 150 MHz.

downfield shift of C-10 ($\Delta\delta_C$ + 31.4). Furthermore, analysis of the ROESY data (Fig. 3) indicated that the relative configurations at the stereogenic centers C-2, C-3, C-6, C-10, C-11, and C-14 were consistent with those of **17**. Finally, the experimental ECD spectrum of **18** showed excellent agreement with the calculated ECD spectrum for (2*R*,3*S*,6*S*,10*S*,11*S*,14*S*)-**18** (Fig. 7), permitting the unambiguous determination of the absolute configuration of **18** as 2*R*,3*S*,6*S*,10*S*,11*S*,14*S*.

Hyperperin S (**19**) was assigned the molecular formula $C_{20}H_{28}O_2$, as indicated by its HR-ESI-MS sodium adduct ion peak at *m/z* 323.1983 $[M + Na]^+$ (Calcd. 323.1982) and supported by ^{13}C NMR data, which corresponded to seven indices of hydrogen deficiency. The ^{1}H and ^{13}C NMR spectra of **19** (Tables 5 and 6) showed signals similar to those of **25** [25]. The major difference was the presence of a 2,6-epoxide moiety in **19**, evidenced by the downfield shifts of the C-2 ($\Delta\delta_C$ + 24.3) and C-6 ($\Delta\delta_C$ + 31.5) signals. This finding was further corroborated by key HMBC correlations (Fig. 2) from H_2-1 (δ_H 2.82, d, *J* = 14.8 Hz; 1.19, d, *J* = 14.8 Hz) and H_2-5 (δ_H 2.17, m; 1.81, m) to both C-2 (δ_C 72.0) and C-6 (δ_C 74.4), from H_2-16 (δ_H 5.02, d, *J* = 1.8 Hz; 4.86, d, *J* = 1.8 Hz) to C-2, and from H_3-17 (δ_H 1.79, s) to C-6. ROESY correlations (Fig. 3) of H_3-18 with H_3-19, and of H-10 with H-14 indicated that H_3-18 was arbitrarily assigned as *α*-oriented, while H-10 and H-14 were determined to be *β*-oriented. However, the ROESY spectrum couldn't provide information to establish the relative configurations at C-2 and C-6. Fortunately, single crystals of **19** suitable for X-ray crystallographic analysis using Cu Kα radiation were successfully obtained. Then, the X-ray data confirmed the planar structure and determined the relative configuration with a Flack parameter of 0.5(3). As shown in Fig. 7, the experimental ECD spectrum of **19** matched well with the calculated one for 2*R*,6*R*,10*R*,11*S*,14*S*-**19**, unambiguously allowing the establishment of the absolute configuration of **19** to be 2*R*,6*R*,10*R*,11*S*,14*S*.

Hyperperin T (**20**) has the molecular formula $C_{20}H_{30}O_3$ with one more oxygen atom than **9**, as determined by (+)-HR-ESI-MS and ^{13}C NMR data. A comparison of the 1D NMR data (Tables 5 and 6) of **20** with those of **9** demonstrated that **20** possesses a framework highly similar to that of **9**. The main differences between them were the presence of a 6,7-epoxide unit [δ_C 74.6 (C-6) and 65.4 (C-7)] and the lack of the terminal double bond at C-7 and C-17 in **20**. This deduction was confirmed HMBC correlations (Fig. 2) from H-2 (δ_H 3.02, br d, *J* = 13.5 Hz), H-8 (δ_H 4.13, br d, *J* = 5.7 Hz), and H_3-17 (δ_H 1.29, s) to both C-6 and C-7. The relative configurations of H-2, H-8, H-10, H-11, and H-14 were identical to those of **9**, as evidenced by their similar ROESY correlations (Fig. 3). The *α*-orientation of the 6,7-epoxide group was supported by ROESY correlations of H_3-17 with H-5b and H-10, of H-10 with H-1b. Finally, a direct comparison between the calculated and experimental ECD spectra of **20** (Fig. 7) unambiguously established its absolute configuration as 2*S*,6*S*,7*R*,8*R*,10*R*,11*S*,14*S*.

Hyperperin U (**21**), a white amorphous powder, possess a molecular formula of $C_{20}H_{30}O_3$, as determined by HR-ESI-MS (*m/z* 341.2088 $[M + Na]^+$, Calcd. for $C_{20}H_{30}O_3Na$, 341.2087). The IR spectrum exhibited absorption bands at 3440, 1736, and 1675 cm^{-1}, which were attributed to OH, C=O, and C=C functional groups, respectively. The ^{1}H and ^{13}C NMR spectra (Tables 5 and 6) showed resonances similar to those of **3**. The major differences included the presence of an aliphatic methine at C-7 and a ketone carbonyl group at C-8 in **21**, replacing the trisubstituted double bond between C-7 and C-8 in **3**. This deduction was assigned based on HMBC correlations (Fig. 2) from H-7 (δ_H 2.29, m) and H_3-17 (δ_H 1.12, d, *J* = 7.0 Hz) to C-8 (δ_C 216.8), as well as

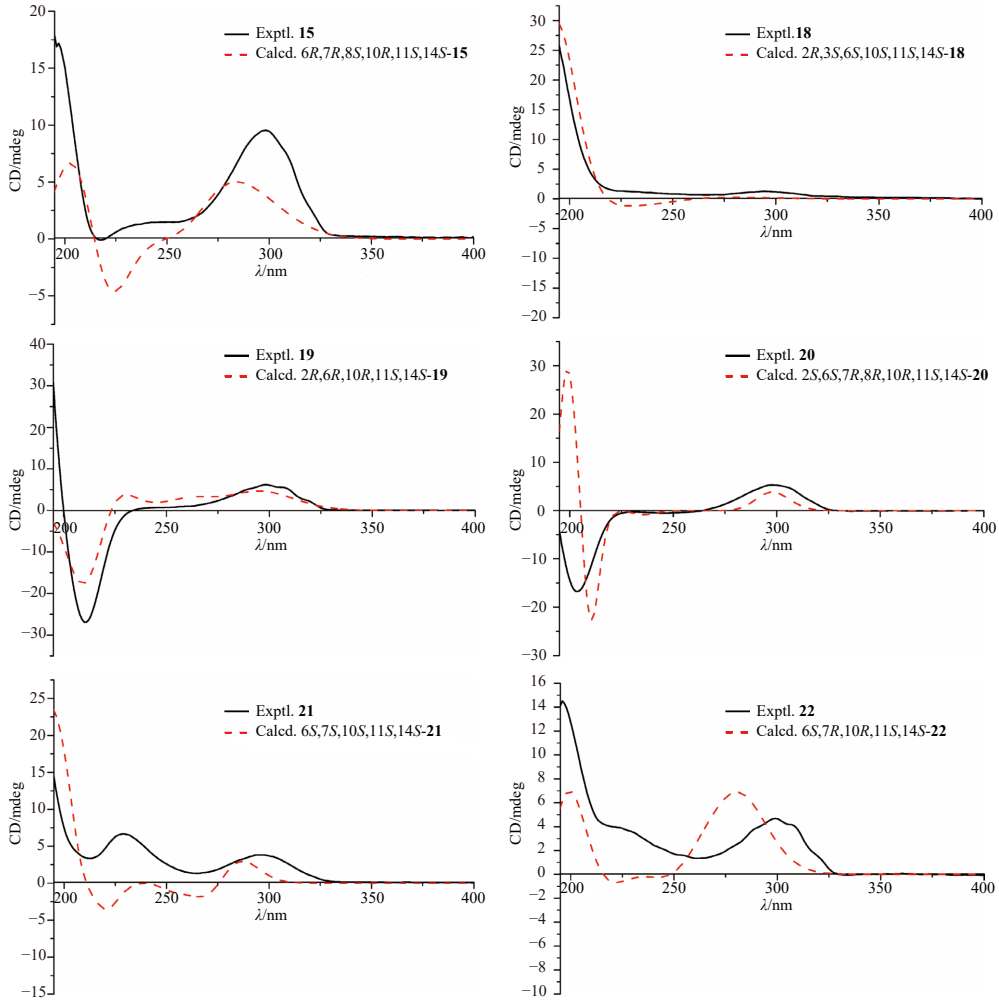


Fig. 7 Experimental and calculated ECD spectra of **15**, **18**-**22**.

^{1}H-^{1}H COSY correlations between H-7 and H_3-17. ROESY correlations (Fig. 3) between H-6/H_3-17, H-6/H_3-18, H_3-18/H_3-20, and 10-OH/H-14 indicated that H-6, H_3-17, and H_3-18 are α-oriented, whereas 10-OH and H-14 are β-oriented. Lastly, the absolute configuration of **21** was determined to be 6*S*,7*S*,10*S*,11*S*,14*S* by comparing its theoretical and experimental ECD spectra (Fig. 7).

Hyperperin V (**22**) was obtained as a white amorphous powder. Its molecular formula, $C_{20}H_{30}O_2$, was determined based on HR-ESI-MS and ^{13}C NMR data. The IR absorption bands at 1737 and 1696 cm^{-1} indicated the presence of carbonyl and olefinic groups, respectively. Compound **22** displayed closely similar 1D NMR data (Tables 5 and 6) to those of **21**, with the key difference being the absence of an additional hydroxyl group at C-10 in **22**. This deduction was confirmed by the upfield shift of the C-10 resonance ($\Delta\delta_C$ -36.7), as well as key HMBC correlations (Fig. 2) from H-10 (δ_H 2.45, m) to C-8 (δ_C 214.9), C-11 (δ_C 49.9), C-12 (δ_C 221.3), and C-18 (δ_C 20.2). ROESY correlations (Fig. 3) of H-1a/H_3-18, H-6/H_3-18, H_3-18/H_3-20, and H-10/H-1b indicated the α-orientations of H-6 and H_3-18, as well as the β-orientations of H-10 and H-14. Furthermore, the C-6 signal was deshielded by $\Delta\delta_C$ + 1.1, whereas C-7, C-8, and C-17 were shielded by $\Delta\delta_C$ -5.5, -1.9, and -5.0, respectively, indicating that the configuration at C-7 in **22** was opposite to that in **21**. The calculated ECD spectrum of **22** (Fig. 7) matched well with the experimental spectrum, allowing the unambiguous assignment of the absolute configuration of **22** as 6*S*,7*R*,10*R*,11*S*,14*S*.

Hyperperin W (**23**) has the molecular formula $C_{20}H_{30}O_3$ with one more oxygen atom than **22**, as determined by (+)-HR-ESI-MS and ^{13}C NMR data. Interpretation of the IR spectrum indicated the presence of typical hydroxyl (3447 cm^{-1}), carbonyl (1737 cm^{-1}), and olefinic (1695 cm^{-1}) functionalities. The ^{1}H and ^{13}C NMR data of **23** (Tables 5 and 6) were similar to those of **22**, except for the presence of one more hydroxyl group in **23**. HMBC correlations (Fig. 2) from H-6 (δ_H 2.65, m) and H_3-17 (δ_H 1.35, s) to C-7 (δ_C 81.6) led to the assignment of the additional hydroxyl group at C-7. The relative configurations at all stereogenic centers of **23** were consistent with those of **22**, as determined by ROESY spectroscopic analysis (Fig. 3). Finally, the absolute configuration of **23** was assigned as 6*R*,7*S*,10*R*,11*S*,14*S* by comparison of its experimental ECD spectrum with that of **22** (Fig. 5).

Hyperperin X (**24**) was isolated as colorless crystals. Its HR-ESI-MS data (*m/z* 325.2136 [M + Na]$^+$, Calcd. for $C_{20}H_{30}O_2Na$, 325.2138) suggested that **24** shares the identical molecular formula, $C_{20}H_{30}O_2$, as **22**. The ^{1}H and ^{13}C-NMR data of **24** (Tables 5 and 6) were highly similar to those of **22**, with the prominent difference being that the double bond between C-2 and C-3 in **22** shifted to C-1 and C-2 in **24**. This finding was confirmed by key HMBC correlations (Fig. 2) from H-3 (δ_H 2.51, m) and H-6 (δ_H 3.54, m) to both C-1 (δ_C 129.8) and C-2 (δ_C 152.0), from H_2-4 (δ_H 1.75, m; 1.27, m) and H_3-16 (δ_H 0.97, d, *J* = 7.1 Hz) to C-2, and from H-10 (δ_H 2.64, ddd, *J* = 12.4, 7.9, 2.7 Hz) and H_3-18 (δ_H 1.21, s) to C-1. ROESY correlations (Fig. 3) of H-6/H_3-18, H-10/H_3-17, H_3-16/H_3-17 and H_3-18/H_3-20 indicated the α-orientations of H-6 and H_3-18, while the β-orientations of H-10, H-14, H_3-16, and H_3-17. Ultimately, single-crystal X-ray crystallography analysis using Cu Kα radiation yielded a Flack parameter of 0.03(4), which unambiguously established the absolute configuration of **24** as 3*S*,6*S*,7*R*,10*R*,11*R*,14*S* (Fig. 6).

Table 6 ^{1}H NMR spectroscopic data of **19**–**24** in acetone-d_6 (J in Hz).

Position	19[a]	20[a]	21[a]	22[b]	23[a]	24[a]
1a	2.82, d (14.8)	1.45, t (13.5)	2.45, d (14.0)	2.32, d (9.5)	2.60, d (15.0)	5.71, br s
1b	1.19, d (14.4)	1.32, dd (13.5, 2.9)	2.06, d (14.0)	2.10, d (9.5)	1.89, d (15.0)	
2		3.02, br d (13.5)				
3						2.51, m
4a	2.26, m	2.40, m	2.22, m	2.27, m	2.37, m	1.75, m
4b	2.15, m	2.36, m	2.22, m	2.13, m	2.08, m	1.27, m
5a	2.17, m	2.41, m	2.14, m	1.94, m	2.01, m	3.20, t (12.6)
5b	1.81, m	1.56, m	1.35, m	1.69, m	1.89, m	2.56, dd (12.6, 2.7)
6			2.96, m	3.10, br s	2.65, m	3.54, m
7			2.29, m	2.81, m		2.96, m
8	5.56, br s	4.13, br d (5.7)				
9a	2.53, m	2.07, m	3.52, d (11.9)	3.00, t (12.2)	3.05, t (12.4)	2.40, dd (6.2, 4.3)
9b	2.46, m	2.01, m	2.55, d (11.9)	2.57, d (12.2)	2.78, dd (12.4, 2.6)	2.40, dd (6.2, 4.3)
10	2.75, ddd (13.1, 7.4, 3.7)	2.54, m		2.45, m	2.70, m	2.64, ddd (12.4, 7.9, 2.7)
13a	2.39, dd (18.7, 1.8)	2.51, dd (17.4, 9.4)	2.45, m	2.40, m	2.44, dd (19.0, 1.9)	1.82, m
13b	2.23, m	2.20, dd (17.4, 1.0)	2.45, m	2.33, m	2.31, dd (19.0, 9.1)	1.82, m
14	2.06, m	2.15, m	2.02, m	2.01, m	2.08, m	2.08, m
15	1.85, m	1.91, m	1.93, m	1.77, m	1.82, m	1.83, m
16a	5.02, d (1.8)	4.85, br s	1.66, s	1.47, s	1.45, s	0.97, d (7.1)
16b	4.86, d, (1.8)	4.82, br s				
17	1.79, s	1.29, s	1.12, d (7.0)	1.04, d (3.5)	1.35, s	1.08, d (7.1)
18	0.90, s	1.24, s	0.92, s	1.03, s	0.98, s	1.21, s
19	0.97, d (6.8)	0.94, d (6.9)	1.08, d (6.6)	1.00, d (6.6)	1.01, d (6.6)	1.01, d (6.6)
20	0.83, d (6.8)	0.73, d (6.9)	0.95, d (6.6)	0.89, d (6.6)	0.90, d (6.6)	0.88, d (6.6)
7-OH					4.01, s	
8-OH		3.15, br s				
10-OH			4.27, s			

[a]Recorded at 500 MHz, [b]Recorded at 600 MHz.

2.2. Proposed biosynthetic pathway

The plausible biosynthetic pathway for compounds **1** and **2** begins with geranylgeranyl pyrophosphate (GGPP) (Scheme 1), which undergoes enzyme-catalyzed cyclization and the release of pyrophosphate (OPP) to form a tricyclic carbocation intermediate **i** [35]. This intermediate then undergoes a 1,5-hydride shift, yielding intermediate **ii**, which subsequently undergoes further cyclization to generate the tricyclic carbocation **iii**. From intermediate **iii**, two tricyclic intermediates **iv** and **v**, are formed through deprotonation at different sites. These intermediates **iv** and **v** are then oxidized to introduce a hydroxyl group at the C-10 position, resulting in **3** and **7**, respectively. The hydroxyl groups in **3** and **7** lose a proton, forming carbocation intermediates **vi** and **vii**, which subsequently undergo deprotonation and cyclization rearrangement to produce **2** and **1**, respectively.

2.3. T-type calcium channel inhibitory

The effects of selected compounds from series **1**–**4**, **6**–**8**, **10**–**11**, **15**, **19**, **20**, **22**, **24**, and **25** on the $Ca_v3.1$ voltage-gated calcium channel were investigated. At a concentration of 25 μmol·L^{-1}, compounds **1**, **2**, **3**, **7**, and **25** exhibited significant inhibition of $Ca_v3.1$ currents, whereas the remaining compounds showed only weak activity (Fig. 8). To evaluate the subtype selectivity of **1**, **2**, **3**, **7**, and **25** on T-type calcium channels, a single concentration (25 μmol·L^{-1}) of each compound was applied to $Ca_v3.2$ and $Ca_v3.3$ channels. The results revealed that, at the tested concentration, compounds **1**, **2**, **3**, and **25** were selective for $Ca_v3.1$, whereas **7** showed no statistically significant differences in inhibition rates among $Ca_v3.1$, $Ca_v3.2$, and $Ca_v3.3$, indicating low selectivity at this concentration (Fig. 9). Based on these selective results, the inhibitory effects of active compounds **1**, **2**, **3**, **7**, and **25** on $Ca_v3.1$ were further evaluated. The results revealed that the inhibitory effects of these five compounds were dose-dependent, with IC_{50} values of 15.06 ± 1.19 μmol·L^{-1} (**1**), 9.00 ± 1.04 μmol·L^{-1} (**2**), 6.04 ± 0.67 μmol·L^{-1} (**3**), 14.00 ± 1.20 μmol·L^{-1} (**7**), and 6.26 ± 0.82 μmol·L^{-1} (**25**) (Fig. 10A). As a positive control, mibefradil effectively inhibited $Ca_v3.1$ currents, displaying an IC_{50} value of 2.11 ± 0.67 μmol·L^{-1} (Fig. 10B). Upon depolarization of the $Ca_v3.1$ channel to −40 mV to evoke peak currents, application of varying concentrations of **1**, **2**, **3**, **7**, and **25**

resulted in concentration-dependent inhibition, further confirming their inhibitory effect on $Ca_v3.1$ (Figs. 10C–10G). Preliminary structure-activity relationship analysis revealed that the C-12 carbonyl group acts as an essential pharmacophore. Reduction of this carbonyl moiety in **8**, **12**, and **17**, as well as its acetylation in **4**, markedly diminished bioactivity. The C-7/C-8 double bond was found to be critical for maintaining potent biological activity. Functional modifications at this position, including hydroxylation in **9** and **20**, carbonylation in **21**–**24**, and epoxidation in **10**, **11**, and **13**–**16**, remarkably diminished bioactivity. Additionally, excessive oxidative modifications and C-2 hydroxylation of the parent skeleton led to decreased biological activity. Specifically, C-2 hydroxylation in **6**, 2,3-epoxidation in **18**, and 2,6-epoxidation in **19** all produced an obvious activity-reducing effect. Moreover, ring system rearrangement and the introduction of a cyclopropane moiety significantly enhanced bioactivity, as exemplified by **1** and **2**, which possess a 5/7/5/3 tetracyclic skeleton.

3. Conclusions

In conclusion, this study presents the isolation and identification of twenty-five fusicoccane diterpenoids from the methanol extract of *H. purpurea*, with twenty-four of these being newly discovered compounds. Notably, compounds **1** and **2** possess an unreported tetracyclic carbon framework characterized by a 5/7/5/3 ring system. Additionally, compounds **19** and **20** represent the first examples of fusicoccane diterpenoids containing epoxy groups at C-2/C-6 and C-6/C-7, respectively. The identification of these unique fusicoccane diterpenoids highlights the remarkable structural diversity of diterpenoids found in *Hypoestes* genus. In biological evaluations, five compounds (**1**, **2**, **3**, **7**, and **25**) exhibited strong inhibitory effects on $Ca_v3.1$ channels. Collectively, these results not only expand the known structural diversity of fusicoccane diterpenoids derived from *Hypoestes* species but also offer promising lead compounds for the development of therapeutics targeting $Ca_v3.1$ channels.

4. Experimental

4.1. General experimental procedures

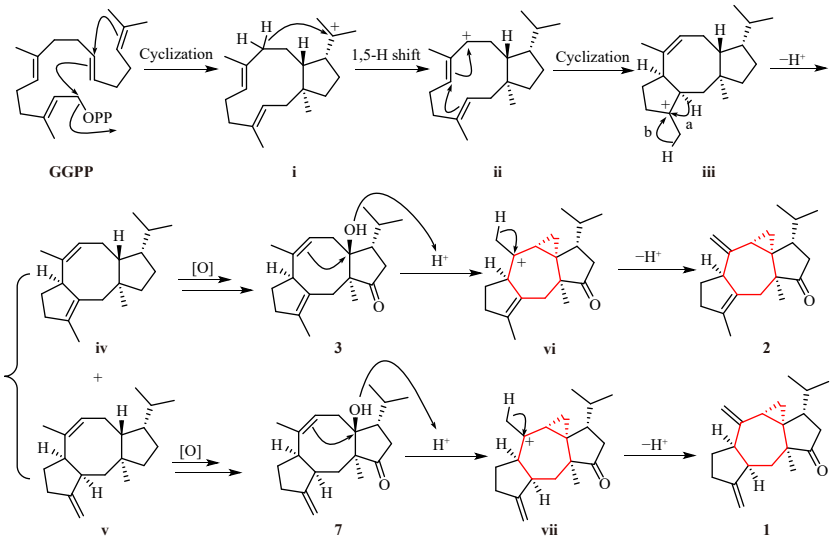
One-dimensional (1D) and two-dimensional (2D) nuclear magnetic resonance (NMR) spectra were acquired on Bruker spectrometers operating at Avance III-500 or AV-600 MHz, with chemical shifts reported in parts per million relative to residual solvent signals. High-resolution electrospray ionization mass spectrometry (HR-ESI-MS) data were collected using either an Agilent 6540 UHD Accurate-Mass Q-TOF or a Shimadzu UPLC-IT-TOF spectrometer. Single-crystal diffractions were collected on a D8 Quest diffractometer using Cu Kα radiation. Ultraviolet (UV) and electronic circular dichroism (ECD) spectra were recorded on an Applied Photophysics spectropolarimeter. Infrared (IR) spectra were obtained on a Thermo Nicolet iS10 spectrophotometer employing KBr pellets. Optical rotations were measured with an Autopol VI polarimeter. Melting points were determined with an X-4 micro-melting point apparatus. Semipreparative high-performance liquid chromatography (HPLC) was conducted on an Agilent 1260 instrument equipped with a UV detector and a Zorbax SB-C_{18} column (Agilent, 5 μm, 9.4 mm × 150 mm). Medium-pressure liquid chromatography (MPLC) was carried out using a Lisui EZ Purify III System (Shanghai LiSui Chemical Engineering Co., Ltd., Shanghai, China). Column chromatography (CC) separations utilized reversed-phase C_{18} gel (40–63 μm, Merck, Darmstadt, Germany) and silica gel (100–200 mesh and 200–300 mesh, Qingdao Marine Chemical Inc., Qingdao, China). Thin-layer chromatography (TLC) was performed on silica gel GF_{254} plates (SiO_2; Qingdao Haiyang Chemical Factory, Qingdao, China), with visualization achieved by heating the plates after spraying with 10% H_2SO_4 in ethanol (*V*/*V*). All solvents were distilled prior to use in experiments.

4.2. Plant material

The aerial parts of *Hypoestes purpurea* were collected in July 2019 from Kunming Botanical Garden, Yunnan Province, China. The plant material was authenticated by Professor Xiao Cheng of the Kunming Institute of Botany, Chinese Academy of Sciences. A voucher specimen (No. 20190701m) has been deposited at the State Key Laboratory of Phytochemistry and Plant Resources in West China, Kunming Institute of Botany, Chinese Academy of Sciences.

4.3. Extraction and isolation.

The air-dried aerial parts of *H. purpurea* (10 kg) were pulverized and exhaustively extracted with methanol (MeOH, 50 L × 4) at ambient temperature (25 ± 2 °C), with each extraction step lasting 48 h. After solvent evaporation under reduced pressure, the resultant crude extract was suspended in distilled water and



Scheme 1 Plausible biosynthetic pathway for compounds **1** and **2**.

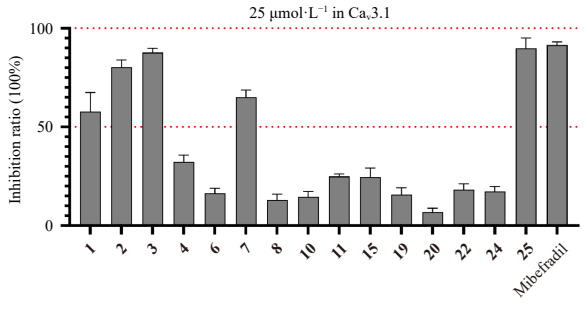


Fig. 8 Inhibitory effects of compounds **1**–**4**, **6**–**8**, **10**, **11**, **15**, **19**, **20**, **22**, **24**, **25** and the positive control (Mibefradil) on the currents of the Ca$_v$3.1 low-voltage-gated calcium channel at 25 μmol·L^{-1}. All data are represented as mean ± SD ($n \geq 3$).

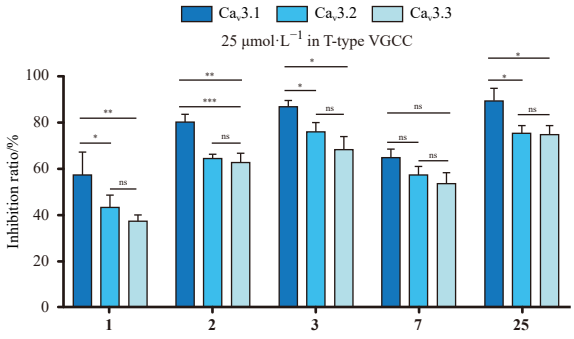


Fig. 9 Selectivity of compounds **1**, **2**, **3**, **7**, and **25** for Ca$_v$3.1, Ca$_v$3.2, and Ca$_v$3.3 at a concentration of 25 μmol·L^{-1}. All data are presented as mean ± SD (n ≥ 3). Statistical comparisons between two groups were performed using a two-tailed unpaired Student's *t*-test. ns: not statistically significant; $^{*}P < 0.05$, $^{**}P < 0.01$, $^{***}P < 0.001$.

successively partitioned against ethyl acetate (EtOAc). The EtOAc-soluble fraction (1.4 kg) was subjected to silica gel CC, eluting with a petroleum ether (PE)–acetone gradient (1∶0–0∶1, *V*/*V*) to afford eight fractions (Fr.1–Fr.8). Fr.2 (151 g) was further chromatographed on a silica gel CC, eluting with PE–EtOAc (300∶1–1∶1, *V*/*V*) to yield seven subfractions (Fr.2.1–Fr.2.7). Fr.2.2 (7.2 g) was further separated by MPLC over an RP-C_{18} gel (MeOH–H_2O, 80∶20–100∶0, *V*/*V*) to obtain ten subfractions (Fr.2.2.1–Fr.2.2.10). Fr.2.2.1 (1.8 g) was purified by silica gel CC with PE–EtOAc (200∶1–15∶1, *V*/*V*) to give six subfractions (Fr.2.2.1.1–Fr.2.2.1.6). Fr.2.2.1.2 (869 mg) was subjected to silica gel CC eluting with PE–acetone (500∶1–20∶1, *V*/*V*) to afford nine subfractions (Fr.2.2.1.2.1–Fr.2.2.1.2.9). Compounds **10** (12.5 mg) and **24** (15.3 mg) was isolated from Fr.2.2.1.2.1 (257 mg) by silica gel CC, eluting with PE–EtOAc (150∶1–6∶4, *V*/*V*). Compounds **2** (6 mg, t_R = 11.5 min) and **4** (18 mg, t_R = 19.2 min) were purified from Fr.2.2.1.2.3 (67 mg) *via* semipreparative HPLC, using an isocratic mobile phase of MeOH–H_2O (90∶10, *V*/*V*). Fr.2.2.1.2.4 (30 mg) was further purified by semipreparative HPLC (MeOH–H_2O, 88∶12, *V*/*V*) to afford **1** (11.4 mg, t_R = 14.6 min). Compound **8** (8.0 mg, t_R = 12.3 min) was obtained from Fr.2.2.1.2.5 (90 mg) by semipreparative HPLC, using an isocratic mobile phase of acetonitrile (MeCN)–H_2O (81∶19, *V*/*V*). Fr.2.2.2 (1.6 g) was separated by silica gel CC with PE–EtOAc (100∶1–6∶4, *V*/*V*) to give seven subfractions (Fr.2.2.2.1–Fr.2.2.2.7). Compound **22** (9.6 mg, t_R = 33.2 min) were purified from Fr.2.2.2.3 (29 mg) *via* semipreparative HPLC with MeCN–H_2O (51∶49, *V*/*V*). Fr.2.2.2.5 (92 mg) was subjected to semipreparative HPLC with MeOH–H_2O (75∶25, *V*/*V*) to yield **15** (8.3 mg, t_R = 11.9 min) and **19** (6.7 mg, t_R = 13.2 min). Compound **25** (8.5 mg, t_R = 20.9 min) was isolated from Fr.2.2.2.7 (127 mg) by semipreparative HPLC with MeOH–H_2O (67∶33, *V*/*V*). Fr.3 (100 g) was fractionated by MPLC over an RP-C_{18} gel, using a gradient elution of MeOH–H_2O (60∶40–100∶0, *V*/*V*), to yield twelve subfractions (Fr.3.1–Fr.3.12). Fr.3.2 (14.0 g) was further subjected by silica gel CC using PE–EtOAc (250∶1–9∶1, *V*/*V*), affording six subfractions (Fr.3.2.1–Fr.3.2.6). Purification of Fr.3.2.2 (16 mg) *via* semipreparative HPLC (MeOH–H_2O, 57∶43, *V*/*V*) yielded **23** (1.8 mg, t_R = 25.1 min). Compounds **7** (18 mg, t_R = 6.3 min), **13** (1.8 mg, t_R = 9.5 min), and **20** (21.2 mg, t_R = 6.8 min) were isolated from Fr.3.2.3 (160 mg) by semipreparative HPLC purification using MeCN–H_2O (40∶60, *V*/*V*). Fr.3.2.4 (56 mg) was purified by semipreparative HPLC (MeCN–H_2O, 38∶62, *V*/*V*) to give **16** (1.6 mg, t_R = 30.6 min). Compound **11** (7.8 mg, t_R = 16.7 min) was purified from Fr.3.2.6 (40 mg) *via* semipreparative HPLC (MeCN–H_2O, 40∶60, *V*/*V*). Fr.3.6 (360 mg) was fractionated by silica gel CC using PE–EtOAc (100∶1–9∶1, *V*/*V*) to produce six subfractions (Fr.3.6.1–Fr3.6.6). Further purification of Fr.3.6.2 (79 mg) by silica gel CC with PE–acetone (200∶1–40∶1, *V*/*V*) afforded **9** (1.8 mg) and **21** (1.7 mg). Semipreparative HPLC purification of Fr.3.6.4 (35 mg) with MeOH–H_2O (65∶35, *V*/*V*) yielded **12** (1.6 mg, t_R = 20.4 min). Compound **6** (9.3 mg, t_R = 16.0 min) was isolated from Fr.3.6.5 (21 mg) by semipreparative HPLC (MeOH–H_2O, 75∶25, *V*/*V*). Fr.3.7 (16 g) was subjected by silica gel CC eluting with PE–EtOAc (100∶1–9∶1, *V*/*V*) to give ten subfractions (Fr.3.7.1–Fr.3.7.10). Compound **3** (15 mg, t_R = 19.6 min) was purified from Fr.3.7.2 (126 mg) *via* semipreparative HPLC (MeCN–H_2O, 60∶40, *V*/*V*). Fr.3.7.3 (75 mg) was subjected to semipreparative HPLC with

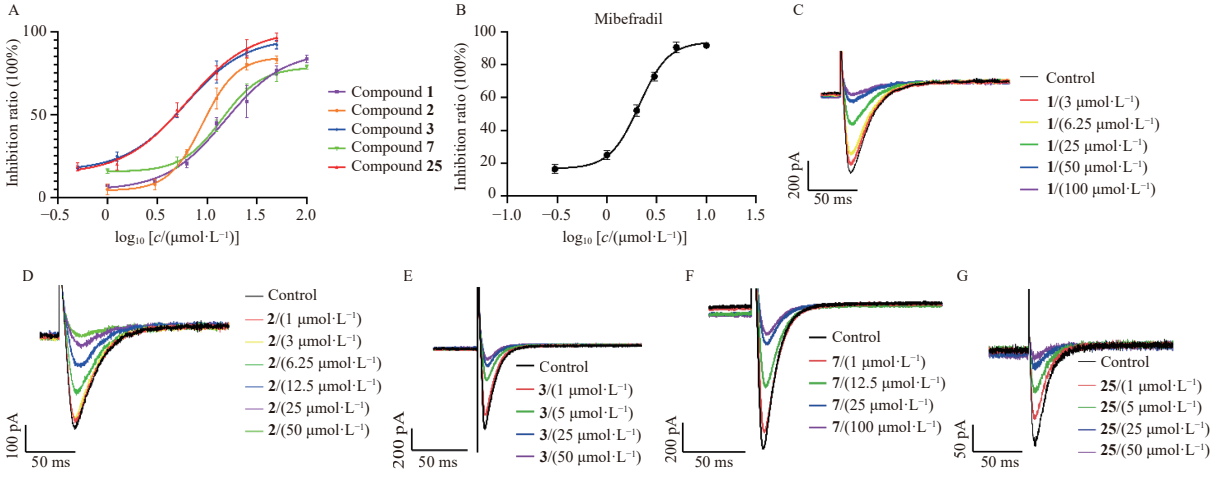


Fig. 10 Effects of compounds on the electrophysiological properties of recombinant Ca$_v$3.1 channels expressed in HEK293T cells. (A) Dose-response curves showing the concentration-dependent decrease in Ca$_v$3.1 peak currents induced by **1**, **2**, **3**, **7**, and **25**. Data were fitted using the Hill equation and points represent mean ± SD ($n \geq 3$). (B) Dose-response curve of mibefradil as a positive control. (C-G) Representative whole-cell Ca$_v$3.1 currents elicited by a 150 ms depolarization to –40 mV in the absence (control) and presence of various concentrations of the compounds ($n \geq 3$).

MeCN–H_2O (58∶42) to yield **14** (1.7 mg, t_R = 17.3 min). Fr.3.7.5 (298 mg) was chromatographed on silica gel CC using PE–acetone (50∶1–9∶1, *V*/*V*) to afford four subfractions (Fr.3.7.5.1–Fr.3.7.5.4). Fr.3.7.5.2 (35 mg) was purified by repeat silica gel CC to give **17** (1.5 mg). Semipreparative HPLC purification of Fr.3.7.5.3 (45 mg) with MeOH–H_2O (65∶35, *V*/*V*) yielded **5** (1.7 mg, t_R = 22.5 min). Further purification of Fr.3.7.5.4 (29 mg) *via* semipreparative HPLC (MeOH–H_2O, 72∶28, *V*/*V*) afforded **18** (1.6 mg, t_R = 7.8 min).

*4.3.1. Hyperperin A (**1**)*

White amorphous powder; $[\alpha]_D^{21.3}$ –99.05 (*c* 0.06, MeOH); UV (MeOH) λ_{max} (log ε): 195 (3.94) nm; CD (MeOH) λ_{max} ($\Delta\varepsilon$): 204 (–4.69) nm, 224 (+2.04) nm, 300 (–0.39) nm; IR (KBr) ν_{max} 3428, 3073, 2957, 1739, 1627, 1464, 1387, 1166, 1139, 961, 877 cm^{-1}; ^1H and ^{13}C NMR data (CD_3OD, 500 and 125 MHz) see Tables 1 and 2; HR-ESI-MS (*m/z* 307.2030 [M + Na]$^+$, Calcd. for $C_{20}H_{28}ONa$, 307.2032).

*4.3.2. Hyperperin B (**2**)*

White amorphous powder; $[\alpha]_D^{20.2}$ +17.55 (*c* 0.13, MeOH); UV (MeOH) λ_{max} (log ε): 195 (4.16) nm; CD (MeOH) λ_{max} ($\Delta\varepsilon$): 207 (+8.20) nm, 238 (–1.18) nm; IR (KBr) ν_{max} 3434, 3069, 2952, 2831, 1726, 1461, 1369, 1152, 1018, 910, 878 cm^{-1}; ^1H and ^{13}C NMR data (acetone-d_6, 500 and 125 MHz) see Tables 1 and 2; HR-ESI-MS (*m/z* 307.2032 [M + Na]$^+$, Calcd. for $C_{20}H_{28}ONa$, 307.2032).

*4.3.3. Hyperperin C (**3**)*

White amorphous powder; $[\alpha]_D^{26.2}$ +58.40 (*c* 0.15, MeOH); UV (MeOH) λ_{max} (log ε): 195 (3.93) nm; CD (MeOH) λ_{max} ($\Delta\varepsilon$): 205 (+12.20) nm, 294 (+0.30) nm; IR (KBr) ν_{max} 3489, 2956, 1719, 1616, 1445, 1384, 1187, 1017, 978, 888 cm^{-1}; ^1H and ^{13}C NMR data (acetone-d_6, 500 and 125 MHz) see Tables 1 and 2; HR-ESI-MS (*m/z* 301.2172 [M – H]$^-$, Calcd. for $C_{20}H_{29}O_2$, 301.2173).

*4.3.4. Hyperperin D (**4**)*

White amorphous powder; $[\alpha]_D^{20.3}$ +127.46 (*c* 0.10, MeOH); UV (MeOH) λ_{max} (log ε): 195 (3.98) nm; CD (MeOH) λ_{max} ($\Delta\varepsilon$): 206 (+12.04) nm; IR (KBr) ν_{max} 3411, 2957, 1737, 1661, 1461, 1389, 1242, 1032, 921, 807 cm^{-1}; ^1H and ^{13}C NMR data (CD_3OD, 500 and 125 MHz) see Tables 1 and 2; HR-ESI-MS (*m/z* 353.2450 [M + Na]$^+$, Calcd. for $C_{22}H_{34}O_2Na$, 353.2451).

*4.3.5. Hyperperin E (**5**)*

White amorphous powder; $[\alpha]_D^{26.6}$ +144.18 (*c* 0.10, MeOH); UV (MeOH) λ_{max} (log ε): 195 (4.50) nm; CD (MeOH) λ_{max} ($\Delta\varepsilon$): 197 (+90.51) nm, 216 (–13.07) nm, 235 (+1.52) nm, 298 (+4.51) nm; IR (KBr) ν_{max} 3438, 3071, 2923, 1733, 1720, 1461, 1372, 1148, 1034, 987, 878 cm^{-1}; ^1H and ^{13}C NMR data (acetone-d_6, 500 and 125 MHz) see Tables 1 and 2; HR-ESI-MS (*m/z* 325.2136 [M + Na]$^+$, Calcd. for $C_{20}H_{30}O_2Na$, 325.2138).

*4.3.6. Hyperperin F (**6**)*

White amorphous powder; $[\alpha]_D^{26.7}$ +54.94 (*c* 0.16, MeOH); UV (MeOH) λ_{max} (log ε): 195 (3.91) nm; CD (MeOH) λ_{max} ($\Delta\varepsilon$): 202 (+7.30) nm, 298 (+0.80) nm; IR (KBr) ν_{max} 3496, 3065, 2996, 1736, 1452, 1383, 1191, 1042, 967, 881 cm^{-1}; ^1H and ^{13}C NMR data (acetone-d_6, 500 and 125 MHz) see Tables 1 and 2; HR-ESI-MS (*m/z* 325.2137 [M + Na]$^+$, Calcd. for $C_{20}H_{30}O_2Na$, 325.2138).

*4.3.7. Hyperperin G (**7**)*

White amorphous powder; $[\alpha]_D^{19.3}$ –14.17 (*c* 0.12, MeOH); UV (MeOH) λ_{max} (log ε): 195 (4.37) nm; CD (MeOH) λ_{max} ($\Delta\varepsilon$): 195 (+56.60) nm, 217 (–13.60) nm; IR (KBr) ν_{max} 3504, 3076, 2959, 1741, 1722, 1683, 1652, 1467, 1378, 1167, 1022, 971, 887 cm^{-1}; ^1H and ^{13}C NMR data (acetone-d_6, 500 and 125 MHz) see Tables 2 and 3; HR-ESI-MS (*m/z* 325.2133 [M + Na]$^+$, Calcd. for $C_{20}H_{30}O_2Na$, 325.2138).

*4.3.8. Hyperperin H (**8**)*

White amorphous powder; $[\alpha]_D^{21.5}$ +59.46 (*c* 0.13, MeOH); UV (MeOH) λ_{max} (log ε): 195 (4.26) nm; CD (MeOH) λ_{max} ($\Delta\varepsilon$): 197 (+50.83) nm, 218 (–9.53) nm; IR (KBr) ν_{max} 3320, 2954, 1734, 1655, 1463, 1388, 1180, 1030, 986, 875 cm^{-1}; ^1H and ^{13}C NMR data (acetone-d_6, 500 and 125 MHz) see Tables 2 and 3; HR-ESI-MS (*m/z* 311.2344 [M + Na]$^+$, Calcd. for $C_{20}H_{32}ONa$, 311.2345).

*4.3.9. Hyperperin I (**9**)*

Colorless crystals (MeOH); mp: 145.4–147.0 °C; $[\alpha]_D^{24.4}$ +9.33 (*c* 0.12, MeOH); UV (MeOH) λ_{max} (log ε): 195 (4.03) nm; CD (MeOH) λ_{max} ($\Delta\varepsilon$): 203 (–13.95) nm, 227 (–0.19) nm, 289 (+1.75) nm; IR (KBr) ν_{max} 3416, 3074, 2957, 1719, 1645, 1460, 1389, 1198, 1040, 993, 883 cm^{-1}; ^1H and ^{13}C NMR data (acetone-d_6, 500 and 125 MHz) see Tables 2 and 3; HR-ESI-MS (*m/z* 325.2136 [M + Na]$^+$, Calcd. for $C_{20}H_{30}O_2Na$, 325.2138).

*4.3.10. Hyperperin J (**10**)*

White amorphous powder;$[\alpha]_D^{20.5}$ +52.86 (*c* 0.10, MeOH); UV (MeOH) λ_{max} (log ε): 195 (3.96) nm; CD (MeOH) λ_{max} ($\Delta\varepsilon$): 206 (–1.24) nm, 235 (+0.12) nm, 297 (+2.60) nm; IR (KBr) ν_{max} 3081, 2969, 2918, 1733, 1654, 1464, 1383, 1184, 1056, 946, 884 cm^{-1}; ^1H and ^{13}C NMR data (acetone-d_6, 500 and 125 MHz) see Tables 2 and 3; HR-ESI-MS (*m/z* 325.2137 [M + Na]$^+$, Calcd. for $C_{20}H_{30}O_2Na$, 325.2138).

*4.3.11. Hyperperin K (**11**)*

White amorphous powder; $[\alpha]_D^{26.1}$ –20.78 (*c* 0.11, MeOH); UV (MeOH) λ_{max} (log ε): 195 (3.89) nm; CD (MeOH) λ_{max} ($\Delta\varepsilon$): 204 (–2.39) nm, 233 (+0.06) nm, 291 (+0.74) nm; IR (KBr) ν_{max} 3479, 3075, 2955, 1739, 1731, 1653, 1467, 1381, 1176, 1037, 985, 876 cm^{-1}; ^1H and ^{13}C NMR data (acetone-d_6, 500 and 125 MHz) see Tables 2 and 3; HR-ESI-MS (*m/z* 341.2089 [M + Na]$^+$, Calcd. for $C_{20}H_{30}O_3Na$, 341.2087)

*4.3.12. Hyperperin L (**12**)*

Colorless crystals (MeOH); mp: 112.0–113.0 °C; $[\alpha]_D^{26.3}$ +49.18 (*c* 0.13, MeOH); UV (MeOH) λ_{max} (log ε): 195 (3.98) nm; CD (MeOH) λ_{max} ($\Delta\varepsilon$): 195 (+6.58) nm, 208 (–5.11) nm; IR (KBr) ν_{max} 3436, 2954, 2876, 1738, 1618, 1464, 1379, 1119, 1050, 982, 876 cm^{-1}; ^1H and ^{13}C NMR data (acetone-d_6, 500 and 125 MHz) see Tables 2 and 3; HR-ESI-MS (*m/z* 303.2333 [M – H]$^-$, Calcd. for $C_{20}H_{31}O_2$, 303.2330).

*4.3.13. Hyperperin M (**13**)*

Colorless crystals (MeOH); mp: 164.0–165.6 °C; $[\alpha]_D^{25.0}$ +70.12 (*c* 0.12, MeOH); UV (MeOH) λ_{max} (log ε): 195 (4.29) nm; CD (MeOH) λ_{max} ($\Delta\varepsilon$): 195 (+10.88) nm, 208 (–2.14) nm, 231 (+0.32) nm, 294 (+0.83) nm; IR (KBr) ν_{max} 3493, 2969, 2839, 1744, 1718, 1621, 1465, 1377, 1179, 1021, 959, 871 cm^{-1}; ^1H and ^{13}C NMR data (acetone-d_6, 500 and 125 MHz) see Tables 4 and 5; HR-ESI-MS (*m/z* 341.2088 [M + Na]$^+$, Calcd. for $C_{20}H_{30}O_3Na$, 341.2087).

*4.3.14. Hyperperin N (**14**)*

White amorphous powder; $[\alpha]_D^{26.6}$ +39.06 (*c* 0.14, MeOH); UV (MeOH) λ_{max} (log ε): 195 (3.63) nm; CD (MeOH) λ_{max} ($\Delta\varepsilon$): 195 (+0.89) nm, 205 (–1.78) nm, 298 (+0.60) nm; IR (KBr) ν_{max} 3435, 2955, 1732, 1612, 1454, 1379, 1190, 1063, 973, 876 cm^{-1}; ^1H and ^{13}C NMR data (acetone-d_6, 500 and 125 MHz) see Tables 4 and 5; HR-ESI-MS (*m/z* 325.2139 [M + Na]$^+$, Calcd. for $C_{20}H_{30}O_2Na$, 325.2138).

*4.3.15. Hyperperin O (**15**)*

White amorphous powder; $[\alpha]_D^{22.0}$ +182.40 (*c* 0.13, MeOH);

UV (MeOH) λ_{max} (log ε): 195 (4.12) nm; CD (MeOH) λ_{max} ($\Delta\varepsilon$): 197 (+6.71) nm, 218 (–0.03) nm, 298 (+3.72) nm; IR (KBr) ν_{max} 3435, 2959, 2922, 1736, 1618, 1454, 1374, 1199, 1057, 974, 861 cm^{-1}; ^1H and ^{13}C NMR data (acetone-d_6, 500 and 125 MHz) see Tables 4 and 5; HR-ESI-MS (*m/z* 325.2135 [M + Na]$^+$, Calcd. for $C_{20}H_{30}O_2Na$, 325.2138).

*4.3.16. Hyperperin P (**16**)*

Colorless crystals (MeOH); mp: 133.5–135.3 °C; $[\alpha]_D^{26.4}$ −16.50 (*c* 0.10, MeOH); UV (MeOH) λ_{max} (log ε): 242 (4.16) nm; CD (MeOH) λ_{max} ($\Delta\varepsilon$): 195 (+3.94) nm, 234 (–3.89) nm, 291 (+0.94) nm; IR (KBr) ν_{max} 3471, 2965, 1741, 1459, 1383, 1187, 1076, 936, 833 cm^{-1}; ^1H and ^{13}C NMR data (acetone-d_6, 500 and 125 MHz) see Tables 4 and 5; HR-ESI-MS (*m/z* 339.1930 [M + Na]$^+$, Calcd. for $C_{20}H_{28}O_3Na$, 339.1931).

*4.3.17. Hyperperin Q (**17**)*

Colorless crystals (MeOH); mp: 164.4–166.0 °C; $[\alpha]_D^{20.1}$ + 163.60 (*c* 0.05, MeOH); UV (MeOH) λ_{max} (log ε): 195 (3.87) nm; CD (MeOH) λ_{max} ($\Delta\varepsilon$): 195 (+13.53) nm; IR (KBr) ν_{max} 3399, 2954, 1631, 1447, 1364, 1220, 1093, 905, 823 cm^{-1}; ^1H and ^{13}C NMR data (acetone-d_6, 500 and 125 MHz) see Tables 4 and 5; HR-ESI-MS (*m/z* 327.2296 [M + Na]$^+$, Calcd. for $C_{20}H_{32}O_2Na$, 327.2295).

*4.3.18. Hyperperin R (**18**)*

White amorphous powder; $[\alpha]_D^{20.2}$ +34.77 (*c* 0.13, MeOH); UV (MeOH) λ_{max} (log ε): 195 (4.06) nm; CD (MeOH) λ_{max} ($\Delta\varepsilon$): 195 (+11.46) nm, 295 (+0.56) nm; IR (KBr) ν_{max} 3441, 2934, 1734, 1629, 1463, 1380, 1176, 1020, 930, 837 cm^{-1}; ^1H and ^{13}C NMR data (acetone-d_6, 600 and 150 MHz) see Tables 4 and 5; HR-ESI-MS (*m/z* 341.2090 [M + Na]$^+$, Calcd. for $C_{20}H_{30}O_3Na$, 341.2087).

*4.3.19. Hyperperin S (**19**)*

Colorless crystals (MeOH); mp: 66.0–67.5 °C; $[\alpha]_D^{27.2}$ +201.80 (*c* 0.11, MeOH); UV (MeOH) λ_{max} (log ε): 195 (4.14) nm; CD (MeOH) λ_{max} ($\Delta\varepsilon$): 195 (+15.93) nm, 210 (–13.91) nm, 298 (+3.20) nm; IR (KBr) ν_{max} 2958, 1735, 1659, 1454, 1408, 1385, 1185, 1024, 961, 852 cm^{-1}; ^1H and ^{13}C NMR data (acetone-d_6, 500 and 125 MHz) see Tables 5 and 6; HR-ESI-MS (*m/z* 323.1983 [M + Na]$^+$, Calcd. for $C_{20}H_{28}O_2Na$, 323.1982).

*4.3.20. Hyperperin T (**20**)*

White amorphous powder; $[\alpha]_D^{25.5}$ +68.86 (*c* 0.13, MeOH); UV (MeOH) λ_{max} (log ε): 195 (3.97) nm; CD (MeOH) λ_{max} ($\Delta\varepsilon$): 204 (–9.00) nm, 233 (–0.15) nm, 298 (+2.86) nm; IR (KBr) ν_{max} 3449, 3070, 2951, 1724, 1655, 1472, 1382, 1285, 1183, 982, 871 cm^{-1}; ^1H and ^{13}C NMR data (acetone-d_6, 500 and 125 MHz) see Tables 5 and 6; HR-ESI-MS (*m/z* 341.2087 [M + Na]$^+$, Calcd. for $C_{20}H_{30}O_3Na$, 341.2087).

*4.3.21. Hyperperin U (**21**)*

White amorphous powder; $[\alpha]_D^{26.6}$ +88.02 (*c* 0.10, MeOH); UV (MeOH) λ_{max} (log ε): 195 (4.14) nm; CD (MeOH) λ_{max} ($\Delta\varepsilon$): 195 (+5.37) nm, 213 (+1.24) nm, 229 (+2.47) nm, 264 (+0.49) nm, 296 (+1.41) nm; IR (KBr) ν_{max} 3440, 2963, 1736, 1675, 1455, 1382, 1180, 1029, 976, 894 cm^{-1}; ^1H and ^{13}C NMR data (acetone-d_6, 500 and 125 MHz) see Tables 5 and 6; HR-ESI-MS (*m/z* 341.2088 [M + Na]$^+$, Calcd. for $C_{20}H_{30}O_3Na$, 341.2087).

*4.3.22. Hyperperin V (**22**)*

White amorphous powder; $[\alpha]_D^{26.0}$ +161.00 (*c* 0.10, MeOH); UV (MeOH) λ_{max} (log ε): 195 (3.94) nm; CD (MeOH) λ_{max} ($\Delta\varepsilon$): 196 (+4.43) nm, 262 (+0.41) nm, 299 (+1.43) nm; IR (KBr) ν_{max} 3436, 2961, 2928, 1737, 1696, 1460, 1384, 1145, 1063, 921, 867 cm^{-1}; ^1H and ^{13}C NMR data (acetone-d_6, 600 and 150 MHz) see Tables 5 and 6; HR-ESI-MS (*m/z* 325.2137 [M + Na]$^+$, Calcd. for $C_{20}H_{30}O_2Na$, 325.2138).

*4.3.23. Hyperperin W (**23**)*

White amorphous powder; $[\alpha]_D^{25.4}$ +126.60 (*c* 0.10, MeOH); UV (MeOH) λ_{max} (log ε): 195 (3.83) nm; CD (MeOH) λ_{max} ($\Delta\varepsilon$): 195 (+3.61) nm, 251 (+0.25) nm, 300 (+2.11) nm; IR (KBr) ν_{max} 3447, 2923, 1737, 1695, 1458, 1374, 1097, 972, 872 cm^{-1}; ^1H and ^{13}C NMR data (acetone-d_6, 500 and 125 MHz) see Tables 5 and 6; HR-ESI-MS (*m/z* 341.2089 [M + Na]$^+$, Calcd. for $C_{20}H_{30}O_3Na$, 341.2087).

*4.3.24. Hyperperin X (**24**)*

Colorless crystals (MeOH); mp: 93.5–95.2 °C; $[\alpha]_D^{23.0}$ +73.82 (*c* 0.11, MeOH); UV (MeOH) λ_{max} (log ε): 195 (3.96) nm; CD (MeOH) λ_{max} ($\Delta\varepsilon$): 195 (–4.52) nm, 207 (–0.38) nm, 225 (–3.76) nm, 299 (+1.90) nm; IR (KBr) ν_{max} 3447, 2983, 2870, 1734, 1701, 1673, 1462, 1377, 1109, 1049, 970, 889 cm^{-1}; ^1H and ^{13}C NMR data (acetone-d_6, 500 and 125 MHz) see Tables 5 and 6; HR-ESI-MS (*m/z* 325.2136 [M + Na]$^+$, Calcd. for $C_{20}H_{30}O_2Na$, 325.2138).

*4.4. X-ray diffraction analysis of **9**, **12**, **13**, **16**, **17**, **19**, and **24***

Colorless crystals of compounds **9**, **12**, **13**, **16**, **17**, **19**, and **24** were obtained *via* recrystallization from MeOH at room temperature. X-ray diffraction data were collected on a Bruker APEX DUO diffractometer using graphite monochromater Cu Kα radiation. The structures were solved by direct methods with SHELXS-97, expanded by difference Fourier technique, and refined by full-matrix least-squares on F^2 using SHELXS-97. All non-hydrogen atoms were refined anisotropically. Hydrogen atoms were added to calculated ideal positions and refined using a riding model. The crystallographic data for compounds **9**, **12**, **13**, **16**, **17**, **19**, and **24** have been deposited at the Cambridge Crystallographic Data Centre. These data can be obtained free of charge *via* www.ccdc.cam.ac.uk.

*4.4.1. Crystal data for hyperperin I (**9**)*

$C_{20}H_{30}O_2$, *M*r = 302.44, *a* = 8.7827(18) Å, *b* = 12.373(3) Å, *c* = 15.631(3) Å, α = 90°, β = 90°, γ = 90°, *V* = 1698.6(6) Å^3, *T* = 100.(2) K, space group *P*212121, *Z* = 4, μ(Cu Kα) = 0.571 mm^{-1}, 17596 reflections measured, 3318 independent reflections (R_{int} = 0.0512). The final R_1 values were 0.0319 ($I > 2\sigma(I)$). The final $wR(F^2)$ values were 0.0835 ($I > 2\sigma(I)$). The final R_1 values were 0.0338 (all data). The final $wR(F^2)$ values were 0.0853 (all data). The goodness of fit on F^2 was 1.043. Flack parameter = 0.02(7). The crystallographic data of **9** (CCDC number 2529521) were stored at the Cambridge Crystallographic Data Centre.

*4.4.2. Crystal data for hyperperin L (**12**)*

$C_{20}H_{32}O_2$, *M*r = 304.45, *a* = 6.9446(2) Å, *b* = 13.3887(4) Å, *c* = 9.6186(3) Å, α = 90°, β = 102.7370(10)°, γ = 90°, *V* = 872.32(5) Å^3, *T* = 100.(2) K, space group *P*1211, *Z* = 2, μ(Cu Kα) = 0.556 mm^{-1}, 14877 reflections measured, 3396 independent reflections (R_{int} = 0.0389). The final R_1 values were 0.0291 ($I > 2\sigma(I)$). The final $wR(F^2)$ values were 0.0760 ($I > 2\sigma(I)$). The final R_1 values were 0.0292 (all data). The final $wR(F^2)$ values were 0.0760 (all data). The goodness of fit on F^2 was 1.090. Flack parameter = 0.17(4). The crystallographic data of **12** (CCDC number 2529522) were stored at the Cambridge Crystallographic Data Centre.

*4.4.3. Crystal data for hyperperin M (**13**)*

$C_{20}H_{30}O_3$, *M*r = 318.44, *a* = 5.8985(3) Å, *b* = 13.0189(6) Å, *c* = 22.7742(11) Å, α = 90.00°, β = 90.00°, γ = 90.00°, *V* = 1748.88(15) Å3, *T* = 100(2) K, space group *P*212121, *Z* = 4, μ(CuKα) = 0.624 mm^{-1}, 17328 reflections measured, 3442 independent reflections (R_{int} = 0.0860). The final R_1 values were 0.0542 ($I > 2\sigma(I)$). The final $wR(F^2)$ values were 0.1318 ($I > 2\sigma(I)$). The final R_1 values were 0.0572 (all data). The final $wR(F^2)$ values were 0.1350 (all data). The goodness of fit on F^2 was 1.085. Flack parameter =

0.16(12). The crystallographic data of **13** (CCDC number 2529523) were stored at the Cambridge Crystallographic Data Centre.

*4.4.4. Crystal data for hyperperin P (**16**)*

$C_{20}H_{28}O_3$, *M*r = 316.42, *a* = 6.0516(5) Å, *b* = 10.9449(9) Å, *c* = 25.342(2) Å, *α* = 90°, *β* = 90°, *γ* = 90°, *V* = 1678.5(2) Å^3, *T* = 100.(2) K, space group *P*212121, *Z* = 4, *μ*(Cu Kα) = 0.650 mm^{-1}, 25394 reflections measured, 3305 independent reflections (R_{int} = 0.0655). The final R_1 values were 0.0308 ($I > 2\sigma(I)$). The final $wR(F^2)$ values were 0.0775 ($I > 2\sigma(I)$). The final R_1 values were 0.0320 (all data). The final $wR(F^2)$ values were 0.0784 (all data). The goodness of fit on F^2 was 1.042. Flack parameter = 0.01(6). The crystallographic data of **16** (CCDC number 2529530) were stored at the Cambridge Crystallographic Data Centre.

*4.4.5. Crystal data for hyperperin Q (**17**)*

$C_{20}H_{32}O_2$, *M*r = 304.45, *a* = 6.8261(2) Å, *b* = 13.0739(4) Å, *c* = 10.0420(3) Å, *α* = 90°, *β* = 91.1060(10)°, *γ* = 90°, *V* = 896.02(5) Å^3, *T* = 100.(2) K, space group *P*1211, *Z* = 2, *μ*(Cu Kα) = 0.542 mm^{-1}, 16707 reflections measured, 3503 independent reflections (R_{int} = 0.0357). The final R_1 values were 0.0282 ($I > 2\sigma(I)$). The final $wR(F^2)$ values were 0.0724 ($I > 2\sigma(I)$). The final R_1 values were 0.0286 (all data). The final $wR(F^2)$ values were 0.0727 (all data). The goodness of fit on F^2 was 1.049. Flack parameter = 0.12(6). The crystallographic data of **17** (CCDC number 2529525) were stored at the Cambridge Crystallographic Data Centre.

*4.4.6. Crystal data for hyperperin S (**19**)*

$C_{20}H_{28}O_2$, *M*r = 300.42, *a* = 6.9352(6) Å, *b* = 7.1379(5) Å, *c* = 34.632(3) Å, *α* = 90°, *β* = 90°, *γ* = 90°, *V* = 1714.4(2) Å^3, *T* = 100.(2) K, space group *P*212121, *Z* = 4, *μ*(Cu Kα) = 0.566 mm^{-1}, 11272 reflections measured, 3327 independent reflections (R_{int} = 0.1186). The final R_1 values were 0.0833 ($I > 2\sigma(I)$). The final $wR(F^2)$ values were 0.2120 ($I > 2\sigma(I)$). The final R_1 values were 0.1108 (all data). The final $wR(F^2)$ values were 0.2523 (all data). The goodness of fit on F^2 was 1.136. Flack parameter = 0.5(3). The crystallographic data of 1**9** (CCDC number 2529527) were stored at the Cambridge Crystallographic Data Centre.

*4.4.7. Crystal data for hyperperin X (**24**)*

$C_{20}H_{30}O_2$, *M*r = 302.44, *a* = 11.5218(3) Å, *b* = 13.8534(4) Å, *c* = 12.1292(4) Å, *α* = 90°, *β* = 116.3910(10)°, *γ* = 90°, *V* = 1734.25(9) Å^3, *T* = 100.(2) K, space group *P*1211, *Z* = 4, *μ*(Cu Kα) = 0.559 mm^{-1}, 28254 reflections measured, 6815 independent reflections (R_{int} = 0.0306). The final R_1 values were 0.0281 ($I > 2\sigma(I)$). The final $wR(F^2)$ values were 0.0725 ($I > 2\sigma(I)$). The final R_1 values were 0.0287 (all data). The final $wR(F^2)$ values were 0.0730 (all data). The goodness of fit on F^2 was 1.033. Flack parameter = 0.03(4). The crystallographic data of **24** (CCDC number 2529528) were stored at the Cambridge Crystallographic Data Centre.

4.5. ECD computational methods

ECD quantum chemical calculations for compounds **1**–**5**, **8**, **10**, **13**, **15**, and **18**–**22** were carried out using the Gaussian 09 software package [36-38]. Preliminary conformational distribution searches were performed with CONFLEX version 8.0 for conformational analysis. Conformers with Boltzmann populations above 1% were further optimized using density functional theory (DFT) at the B3LYP/6-31G(d,p) level with Gaussian 09. The optimized conformers were then used for ECD calculations at the B3LYP/6-31G(d,p) level within the polarizable continuum model (PCM) of methanol, also using Gaussian 09. The resulting ECD spectra were Boltzmann-averaged and processed with the SpecDis program, applying a half bandwidth of 0.3 eV.

4.6. T-type calcium channel inhibitory assay

4.6.1. Cell cultivation and expression

Human embryonic kidney (HEK) 293T cells (purchased from ATCC) were cultured in DMEM (VivaCell, Shanghai, China) supplemented with 10% newborn calf serum (VivaCell, Shanghai, China) and penicillin (100 U·mL^{-1})/streptomycin (0.1 mg·mL^{-1}) (VivaCell, Shanghai, China) at 37 °C in a humidified atmosphere containing 5% CO_2 [39, 40]. HEK 293T cells were transfected using Lipofectamine 3000 (Invitrogen) with pCDNA3.1-human $Ca_v3.1$/$Ca_v3.2$/$Ca_v3.3$ and pCDNA3.1-eGFP plasmids and used 48 h post-transfection.

4.6.2. Whole-cell voltage-clamp recordings

All recordings were performed at room temperature (25 °C). The cell membrane potential was held at −100 mV. Peak currents of $Ca_v3.1$ and $Ca_v3.2$ were elicited by a 150 ms depolarization from a holding potential of −100 mV to −40 mV at 4 s intervals, whereas $Ca_v3.3$ required the depolarization duration to be extended to 400 ms. Voltage step recordings were elicited by depolarizations −80 mV to +60 mV over 150 ms at 1.5 s intervals. Borosilicate glass micropipettes were pulled to produce a resistance of 2–6 MΩ (P-1000, Sutter Instrument) and filled with an intracellular recording solution containing 130 mmol·L^{-1} CsCl, 2 mmol·L^{-1} $MgCl_2$, 10 mmol·L^{-1} EGTA, 5 mmol·L^{-1} Na-ATP, and 10 mmol·L^{-1} HEPES (pH 7.2 adjusted with CsOH). The extracellular recording solution consisted of 145 mmol·L^{-1} CsCl, 1 mmol·L^{-1} $MgCl_2$, 2 mmol·L^{-1} $CaCl_2$, 10 mmol·L^{-1} glucose, and 10 mmol·L^{-1} HEPES (pH 7.4 adjusted with CsOH). Current signals were amplified using an amplifier (SUTTER IPA-2), passed through a low energy filter at 2 kHz, and then sampled at 10 kHz.

4.6.3. Data analysis and statistics

Data fitting and statistical analyses were performed using GraphPad Prism 8.0. IC_{50} values were determined by fitting the data points to the Hill equation in the form of $Y = I_{Min} + (I_{Max} - I_{Min})/ [1 + 10(\log IC_{50} - c) \times \text{Hillslope}]$. In this equation, IC_{50} represents the concentration at which half-maximal currents are inhibited within the tested concentration range, *c* is the log concentration of compounds, I_{Min} is the minimum stimulation ratio, I_{Max} is the maximum stimulation ratio, and Hillslope is the Hill coefficient. All data are presented as mean ± standard deviation (SD).

Fundings

This work was supported by the National Natural Science Foundation of China (Nos. 22267022 and 82360681), Yunnan Foundamental Research Project (No. 202301AT070266), the Yunnan Fundamental Research-Joint Special Project of Kunming Medical University (No. 202401AY070001-062), Yunnan Revitalization Talent Support Program (No. XDYC-QNRC-2024-180), and First-Class Discipline Team of Kunming Medical University (No. 2024XKTDTS12).

Supplementary data

Supplementary data associated with this article can be requested by sending E-mail to the corresponding authors.

Declaration of competing interest

The authors have no conflict of interest to declare.

References

1 Attali B, Gao ZB. Ion channels research in the post-genomic era. *Acta*

Pharmacol Sin. 2016;37(1):1-3. https://doi.org/10.1038/aps.2015.144.
2 Behrends JC. Evolution of the ion channel concept: the historical perspective. *Chem Rev*. 2012;112(12):6218-6226. https://doi.org/10.1021/cr300349g.
3 Felix R, Corzo-Lopez A, Sandoval A. Voltage-gated ion channels in neuropathic pain signaling. *Life*. 2025;15(6):888. https://doi.org/10.3390/life15060888.
4 Fan JJ, Huang X. Ion channels in cancer: orchestrators of electrical signaling and cellular crosstalk. *Rev Physiol Biochem Pharmacol*. 2022;183:103-133. https://doi.org/10.1007/112_2020_48.
5 Cheng J, Wen J, Wang NX, et al. Ion channels and vascular diseases. *Arterioscler Thromb Vasc Biol*. 2019;39(5):e146-e156. https://doi.org/10.1161/ATVBAHA.119.312004.
6 Kumar P, Kumar D, Jha SK, et al. Ion channels in neurological disorders. *Adv Protein Chem Struct Biol*. 2016;103:97-136. https://doi.org/10.1016/bs.apcsb.2015.10.006.
7 Bagal SK, Brown AD, Cox PJ, et al. Ion channels as therapeutic targets: a drug discovery perspective. *J Med Chem*. 2013;56(3):593-624. https://doi.org/10.1021/jm3011433.
8 Santos R, Ursu O, Gaulton A, et al. A comprehensive map of molecular drug targets. *Nat Rev Drug Discov*. 2017;16(1):19-34. https://doi.org/10.1038/nrd.2016.230.
9 Bajaj S, Ong ST, Chandy KG. Contributions of natural products to ion channel pharmacology. *Nat Prod Rep*. 2020;37(5):703-716. https://doi.org/10.1039/c9np00056a.
10 Yunker AM, McEnery MW. Low-voltage-activated ("T-Type") calcium channels in review. *J Bioenerg Biomembr*. 2003;35(6):533-575. https://doi.org/10.1023/b:jobb.0000008024.77488.48.
11 Zamponi GW, Striessnig J, Koschak A, et al. The physiology, pathology, and pharmacology of voltage-gated calcium channels and their future therapeutic potential. *Pharmacol Rev*. 2015;67(4):821-870. https://doi.org/10.1124/pr.114.009654.
12 Perez-Reyes E. Molecular physiology of low-voltage-activated t-type calcium channels. *Physiol Rev*. 2003;83(1):117-161. https://doi.org/10.1152/physrev.00018.2002.
13 Melgari D, Frosio A, Calamaio S, et al. T-type calcium channels: a mixed blessing. *Int J Mol Sci*. 2022;23(17):9894. https://doi.org/10.3390/ijms23179894.
14 Powell KL, Cain SM, Snutch TP, et al. Low threshold T-type calcium channels as targets for novel epilepsy treatments. *Br J Clin Pharmacol*. 2014;77(5):729-739. https://doi.org/10.1111/bcp.12205.
15 Wang D, Ragnarsson L, Lewis RJ. T-type calcium channels in health and disease. *Curr Med Chem*. 2020;27(19):3098-3122. https://doi.org/10.2174/0929867325666181001112821.
16 Ono K, Iijima T. Cardiac T-type Ca^{2+} channels in the heart. *J Mol Cell Cardiol*. 2010;48(1):65-70. https://doi.org/10.1016/j.yjmcc.2009.08.021.
17 Weiss N, Zamponi GW. T-type calcium channels: from molecule to therapeutic opportunities. *Int J Biochem Cell Biol*. 2019;108:34-39. https://doi.org/10.1016/j.biocel.2019.01.008.
18 Yang YC, Tai CH, Pan MK, et al. The T-type calcium channel as a new therapeutic target for Parkinson's disease. *Pflugers Arch*. 2014;466(4):747-755. https://doi.org/10.1007/s00424-014-1466-6.
19 Matthews LG, Puryear CB, Correia SS, et al. T-type calcium channels as therapeutic targets in essential tremor and Parkinson's disease. *Ann Clin Transl Neurol*. 2023;10(4):462-483. https://doi.org/10.1002/acn3.51735.
20 Zhou FJ, Nian Y, Yan YM, et al. Two new classes of T-type calcium channel inhibitors with new chemical scaffolds from *Ganoderma cochlear*. *Org Lett*. 2015;17(12):3082-3085. https://doi.org/10.1021/acs.orglett.5b01353.
21 Ye YS, Li WY, Du SZ, et al. Congenetic hybrids derived from dearomatized isoprenylated acylphloroglucinol with opposite effects on $Ca_v3.1$ low voltage-gated Ca^{2+} Channel. *J Med Chem*. 2020;63(4):1709-1716. https://doi.org/10.1021/acs.jmedchem.9b02056.
22 Zhou HF, Li WY, Peng LY, et al. Rhynchines A–E: $Ca_v3.1$ calcium channel blockers from *Uncaria rhynchophylla*. *Org Lett*. 2021;23(24):9463-9467. https://doi.org/10.1021/acs.orglett.1c03641.
23 Editorial committee of flora of China, Chinese Academy of Sciences. *Flora of China*. Beijing: Science Pres, 2002.
24 Shen CC, Ni CL, Huang YL, et al. Furanolabdane diterpenes from *Hypoestes purpurea*. *J Nat Prod*. 2004;67(11):1947-1949. https://doi.org/10.1021/np0497402.
25 D'Ambola M, Fiengo L, Chini MG, et al. Fusicoccane diterpenes from *Hypoestes forsskaolii* as heat shock protein 90 (Hsp90) modulators. *J Nat Prod*. 2019;82(3):539-549. https://doi.org/10.1021/acs.jnatprod.8b00924.
26 Yan T, Ding LF, Chen Y, et al. Labdane-type diterpenoids from *Hypoestes phyllostachya* inhibit pancreatic cancer stem cells. *Phytochemistry*. 2025;240:114650. https://doi.org/10.1016/j.phytochem.2025.114650.
27 Wu XD, Luo D, Tu WC, et al. Hypophyllins A–D, labdane-type diterpenoids with vasorelaxant activity from *Hypoestes phyllostachy*a "Rosea". *Org Lett*. 2016;18(24):6484-6487. https://doi.org/10.1021/acs.orglett.6b03388.
28 Wu XD, Ding LF, Li WY, et al. Hypoestins A–D: highly modified fusicoccane diterpenoids with promising $Ca_v3.1$ calcium channel inhibitory activity from *Hypoestes purpurea*. *Org Chem Front*. 2022;9(11):3075-3083. https://doi.org/10.1039/d2qo00265e.
29 Rasoamiaranjanahary L, Marston A, Guilet D, et al. Antifungal diterpenes from *Hypoestes serpens* (Acanthaceae). *Phytochemistry*. 2003;62(3):333-337. https://doi.org/10.1016/s0031-9422(02)00551-4.
30 Al Musayeib NM, Mothana RA, Mohamed GA, et al. Hypoestenonols A and B, new fusicoccane diterpenes from *Hypoestes forskalei*. *Phytochem Lett*. 2014;10:23-27. https://doi.org/10.1016/j.phytol.2014.06.020.
31 Cheng B, Ding LF, Yan T, et al. Hypofolins A–L, ent-labdane diterpenoids from the roots of *Hypoestes phyllostachya* 'Pink Splash'. *Chem Biodivers*. 2018;15(6):e1800124. https://doi.org/10.1002/cbdv.201800124.
32 Muhammad I, Mossa JS, Al-Yahya MA, et al. Hypoestenone: a fusicoccane diterpene ketone from *Hypoestes forskalei*. *Phytochemistry*. 1997;44(1):125-129. https://doi.org/10.1016/S0031-9422(96)00474-8.
33 Andriamihaja B, Martin MT, Rasoanaivo P, et al. A new diterpene from *Hypoestes serpens*. *J Nat Prod*. 2001;64(2):217-218. https://doi.org/10.1021/np0001474.
34 Al-Rehaily AJ, Al-Yahya MA, Mirza HH, et al. Verticillarone: a new seco-fusicoccane diterpenoid ketonepoxide from *Hypoestes verticillaris*. *J Asian Nat Prod Res*. 2002;4(2):117-122. https://doi.org/10.1080/10286020290027399.
35 Tang XW, Zhang F, Zeng T, et al. Enzymatic plasticity inspired by the diterpene cyclase $CotB_2$. *ACS Chem Biol*. 2020;15(10):2820-2832. https://doi.org/10.1021/acschembio.0c00645.
36 Wang YL, Chen J, Zheng WS, et al. New diterpenoids from *Euphorbia wallichii* with antioxidant activity. *Chin J Nat Med*. 2025;23(10):1248-1258. https://doi.org/10.1016/S1875-5364(25)60859-4.
37 Zhang J, Yan JK, Dong HJ, et al. Dimeric sesquiterpenoids with anti-inflammatory activities from *Inula britannica*. *Chin J Nat Med*. 2025;23(8):961-971. https://doi.org/10.1016/S1875-5364(25)60931-9.
38 Cheng HZ, Liu H, Qi XY, et al. Anti-inflammatory and hepatoprotective triterpenoids from the traditional Mongolian medicine *Gentianopsis barbata*. *Chin J Nat Med*. 2025;23(9):1111-1121. https://doi.org/10.1016/S1875-5364(25)60870-3.
39 Gong Y, Liu R, Zha HJ, et al. Analgesic buxus alkaloids with enhanced selectivity for the low-voltage-gated calcium channel $Ca_v3.2$ over $Ca_v3.1$ through a new binding mode. *Angew Chem Int Ed Engl*. 2024;63(1):e202313461. https://doi.org/10.1002/anie.202313461.
40 Li M, Wang XJ, Zhao Q, et al. Bufalin-induced cardiotoxicity: new findings into mechanisms. *Chin J Nat Med*. 2020;18(7):550-560. https://doi.org/10.1016/S1875-5364(20)30065-0.